

## Optical properties of aged Asian aerosols observed over the U.S. Pacific Northwest

E. V. Fischer,<sup>1</sup> D. A. Jaffe,<sup>1,2</sup> N. A. Marley,<sup>3</sup> J. S. Gaffney,<sup>4</sup> and A. Marchany-Rivera<sup>5</sup>

Received 27 January 2010; revised 5 May 2010; accepted 10 June 2010; published 29 October 2010.

[1] A suite of gas-phase and aerosol measurements were made during spring 2008 and spring 2009 at the Mount Bachelor Observatory (2763 masl), located in Oregon. Here we focus on multiwavelength observations of low RH submicron ( $\mu\text{m}$ ) aerosol scattering ( $\sigma_{\text{sp}}$ ) and absorption ( $\sigma_{\text{ap}}$ ), made with an integrating nephelometer and a particle soot absorption photometer. Using a combination of in situ observations, trajectory calculations and satellite observations, we identified seven plumes of Asian origin. These plumes included many of the highest  $\sigma_{\text{sp}}$  ( $34.8 \text{ Mm}^{-1}$ ) and  $\sigma_{\text{ap}}$  ( $5.7 \text{ Mm}^{-1}$ ) hourly average values observed at MBO over the 2008 and 2009 campaigns. Of interest in this analysis is (1) whether the intensive optical properties differ between these seven plumes, (2) whether these differences can be linked to differences in composition, and (3) whether the intensive optical properties change during transpacific transport. Results show that the plumes clustered in terms of their optical properties; plumes hypothesized to contain a large fraction of mineral dust were the most distinct. We observed variability between plumes in the scattering Ångström ( $\text{Å}_s$ ) exponent. The average submicrometer  $\text{Å}_s$  for all seven plumes was significantly larger than the same parameter observed closer to Asia. Therefore, we hypothesize that the aerosol size distribution shifts toward smaller particles during transpacific transport. The average submicrometer low-RH aerosol single scatter albedo ( $\omega$ ) observed at MBO (0.88) was slightly larger than previous observations closer to the Asian coast, and the average backscatter fraction ( $b$ ) was smaller, on the order of 20%.

**Citation:** Fischer, E. V., D. A. Jaffe, N. A. Marley, J. S. Gaffney, and A. Marchany-Rivera (2010), Optical properties of aged Asian aerosols observed over the U.S. Pacific Northwest, *J. Geophys. Res.*, 115, D20209, doi:10.1029/2010JD013943.

### 1. Introduction

[2] Aerosols are an important component of the climate system, and the impact of increased atmospheric aerosol loading due to anthropogenic activities has yet to be fully quantified [Rockström *et al.*, 2009]. Aerosols absorb and scatter solar radiation, and this is known as the aerosol direct effect. The present uncertainty in the global aerosol direct effect is of the same magnitude as the effect itself [Intergovernmental Panel on Climate Change (IPCC), 2007]. Over the past decade, several assessments have highlighted the areas of uncertainties in assessing the global aerosol direct effect. One recurring issue is an incomplete in situ observational record [Diner *et al.*, 2004; Kaufman *et al.*, 2002]. To min-

imize the uncertainties associated with the anthropogenic aerosol effect on climate we need to (1) relate aerosol optical properties to emissions from specific source regions, (2) separate the natural aerosol from the anthropogenic component, and (3) develop a better understanding of how the optical properties of aerosols change with time and processing [Kaufman *et al.*, 2002].

[3] The scattering and absorption properties of atmospheric aerosols consist of the wavelength-dependent scattering coefficient ( $\sigma_{\text{sp}}$ ), the wavelength-dependent absorption coefficient ( $\sigma_{\text{ap}}$ ), and the angular distribution of the scattered light. Both of the coefficients ( $\sigma_{\text{sp}}$  and  $\sigma_{\text{ap}}$ ) can be measured by in situ instruments and have units of inverse length ( $\text{Mm}^{-1}$ ). The  $\sigma_{\text{sp}}$  ( $\sigma_{\text{ap}}$ ) is the product of the aerosol scattering (absorption) cross section and the concentration of scattering (absorbing) particles.

[4] The wavelength dependence of aerosol scattering has historically been parameterized as proportional to  $\lambda^{-\text{Å}_s}$ , where  $\text{Å}_s$  is the aerosol scattering Ångström exponent [Ångström, 1929]. The scattering properties of aerosols are a function of particle size. For large particles, such as sea salt and dust,  $\sigma_{\text{sp}}$  changes little with wavelength, so  $\text{Å}_s$  is small. For small particles, such as those generated by gas-to-particle conversion or directly from combustion,  $\sigma_{\text{sp}}$  decreases rapidly with wavelength, so  $\text{Å}_s$  is larger [Boren and Huffman, 1983]. The

<sup>1</sup>Department of Atmospheric Sciences, University of Washington, Seattle, Washington, USA.

<sup>2</sup>Science and Technology Program, University of Washington Bothell, Bothell, Washington, USA.

<sup>3</sup>Graduate Institute of Technology, University of Arkansas at Little Rock, Little Rock, Arkansas, USA.

<sup>4</sup>Department of Chemistry, University of Arkansas at Little Rock, Little Rock, Arkansas, USA.

<sup>5</sup>Department of Applied Science, University of Arkansas at Little Rock, Little Rock, Arkansas, USA.



**Figure 1.** Location of Mount Bachelor and two other relevant IMPROVE monitoring sites: Mount Hood and Three Sisters Wilderness Area.

aerosol absorption coefficient has been parameterized analogously as proportional to  $\lambda^{-\hat{A}_a}$ , where  $\hat{A}_a$  is the aerosol absorption Ångström exponent.  $\hat{A}_a$  depends on the size, composition, shape and mixing state of the aerosols [Bergstrom et al., 2007]. Determining the spectral variation of aerosol scattering and absorption is important because it allows measurements of  $\sigma_{sp}$  and  $\sigma_{ap}$  at specific wavelengths to be extrapolated over the solar spectrum. The relationship between  $\hat{A}_s$  and  $\hat{A}_a$  varies with aerosol composition, and can be used to stratify in situ data by plume type [Clarke et al., 2007; Yang et al., 2009]. The spectral variation of absorption ( $\hat{A}_a$ ) has been used to separate absorption from dust aerosols from combustion-generated carbonaceous aerosols [Fialho et al., 2005].

[5] Two other important intensive properties can be derived from measurements of  $\sigma_{ap}$ ,  $\sigma_{sp}$ , and the aerosol backscattering coefficient ( $\sigma_{bsp}$ ). The single scatter albedo ( $\omega$ ) is the fraction of total light extinction due to scattering, and the value of  $\omega$  determines whether an aerosol layer causes net heating or cooling [Haywood and Shine, 1995]. The ratio of aerosol scattering directed toward the backward hemisphere to scattering in all directions is called the backscatter ratio ( $b$ ). For specific particle types, the angular distribution of scattering can be approximated from  $b$ , and thus  $b$  can be used to estimate the fraction of incoming solar radiation that aerosols redirect toward space [Marshall et al., 1995].

[6] Atmospheric aerosols in the free troposphere over the west coast of the United States can be broadly classified into three categories by their sources: industrial, dust and biomass burning. Industrial aerosols can have a North American source or they can be advected across the Pacific from Asia [Anderson et al., 1999; Heald et al., 2006; Jaffe et al., 1999]. There is strong evidence that aerosols from East Asia significantly impact air quality and regional climate over North America, especially during spring [VanCuren, 2003; Wuebbles et al., 2007; Yu et al., 2008]. The direct emissions of aerosols and their gas-phase precursors will continue to rise in East Asia due to increases in energy consumption and a continued reliance on coal [Carmichael et al., 2009].

[7] The springtime transport of Asian dust across the Pacific has been well documented [Husar et al., 2001; Jaffe et al., 2003a]. Although Asian dust impacts the United States throughout the year [VanCuren and Cahill, 2002] spring is the preferred season due to the intense frontal activity that allows for lofting and enhanced outflow from Asia. Dust plumes are generally transported higher than pollution plumes, this combined with a lower wet scavenging efficiency can allow up to  $\sim 3$  times more fine dust aerosols to reach the United States from Asia than other types of aerosols [Chin et al., 2007]. The impact of dust is not isolated to large plumes. Approximately 50% of the interannual variability in springtime average  $PM_{2.5}$  in remote areas of the U.S. Pacific Northwest can be explained by year-to-year changes in Asian dust emissions [Fischer et al., 2009].

[8] Biomass burning is one of the largest global sources of accumulation mode ( $<1 \mu\text{m}$  diameter) particles, implying radiative and geochemical impacts [Reid et al., 2004, 2005]. The largest number of fires in the western United States occurs from May to October [Westerling et al., 2003]. However, in the Northern Hemisphere the biomass burning maximum occurs in spring, largely dominated by African and Southeast Asian sources [Duncan et al., 2003]. Siberian biomass burning plumes can travel to western North America and the North American Arctic relatively quickly, on the order of a week, and boreal fires generally take place from May to September [Duncan et al., 2003; Jaffe et al., 2004]. In spring 2008 the Russian boreal forest fire season started unusually early due to low snow amounts (<http://rapidfire.sci.gsfc.nasa.gov/firemaps/>) [Warneke et al., 2009].

[9] Since its establishment, the Mount Bachelor Observatory (MBO) (2763 m amsl) has proven to be well positioned to observe the transpacific transport of Asian industrial, dust and biomass burning plumes [Weiss-Penzias et al., 2007, 2006]. We report here on springtime observations of submicrometer aerosol optical properties from MBO, located in the lower free troposphere over the Pacific Northwest. These observations are valuable for a number of reasons. The submicrometer aerosol observations at MBO integrate aerosol size, shape, chemistry and mixing state, and therefore apply to the entire fine mode aerosol population. Second, the observations at MBO were made over a relatively long time scale ( $>1000$  h for each spring campaign) and with a high enough time resolution to allow separation of plume conditions from background aerosol. We identify seven well-defined plumes of Asian origin and use a variety of supporting in situ data, satellite observations and model analysis to gain information on plume composition. Owing to the close proximity of anthropogenic, biomass burning and dust aerosol sources,

each plume leaving Asia reflects a different mixture of aerosols. Relationships between the observed optical properties are noted for plumes observed at MBO, and we attempt to identify plumes with a large mineral dust component. Finally, the optical properties for the seven plumes observed at MBO are compared to similar observations closer to the Asian source region.

## 2. Methods

### 2.1. Site Description and Sampling Configuration

[10] The observations used in this paper were made in April–May 2008 and April–May 2009 at the Mount Bachelor Observatory (MBO). MBO is located on the summit of a dormant volcano in central Oregon (43.98°N 121.7°W, 2763 m amsl) (Figure 1). Separate aerosol and gas sampling inlets were located 3 m above the roof of the summit lift building, and the instruments were located in a room within the building, situated approximately 15 m below the inlet. The aerosol sample line was situated such that the last 2.5 m were located within the space which was temperature controlled at  $20 \pm 3^\circ\text{C}$ , typically  $10^\circ\text{--}20^\circ\text{C}$  warmer than ambient. The aerosol inlet line was constructed of 0.688" ID conductive tubing. The inlet faced down and there were no sharp bends in the line where aerosols could accumulate. Total flow through the aerosol line was  $\sim 35 \text{ L min}^{-1}$ . Carbon monoxide (CO), ozone ( $\text{O}_3$ ),  $\text{NO}_x$  ( $\text{NO}_x = \text{NO} + \text{NO}_2$ ), PAN and total reactive nitrogen ( $\text{NO}_y$ ) were sampled through a 1/4" internal diameter PFA Teflon line, with a 1  $\mu\text{m}$  Teflon filter located at the inlet. Temperature (T), relative humidity (RH), pressure (P), and wind direction were also measured at the summit. The methods pertaining to the ongoing gas-phase measurements (CO and  $\text{O}_3$ ) have been described previously [Weiss-Penzias *et al.*, 2006]. The methods pertaining to the reactive nitrogen measurements are described separately [Fischer *et al.*, 2010; Reidmiller *et al.*, 2010]. All data are reported in GMT which is 7 h later than local Pacific Daylight Time (GMT = PDT + 7).

### 2.2. Aerosol Measurements

#### 2.2.1. Overview of Aerosol Measurements

[11] The aerosol stream was split approximately 14 m downstream of the inlet into two air streams (both constructed of 0.688" ID conductive tubing), from one a Radiance Research (M903) nephelometer measured midvisible (530 nm) submicrometer dry aerosol scattering. The methods pertaining to the single wavelength scattering measurements have been described previously [Weiss-Penzias *et al.*, 2006].

[12] Multiwavelength submicrometer aerosol light scattering and absorption were measured from the second air stream. An integrating nephelometer (Model 3563, TSI Inc., St. Paul, Minnesota) was used to measure submicrometer dry (RH < 30%) light scattering ( $\sigma_{\text{sp}}$ ) and hemispheric backscattering ( $\sigma_{\text{bsp}}$ ; i.e.,  $90^\circ\text{--}180^\circ$  scattering) at three wavelengths (450, 550, and 700 nm) [Anderson *et al.*, 1996; Heintzenberg and Charlson, 1996]. Backscattering was measured during spring 2009 but not in spring 2008. Preceding the integrating nephelometer was a Berner impactor [Berner *et al.*, 1979] run at  $30 \text{ L min}^{-1}$  and employing a greased substrate to prevent particle bounce. This flow rate gives a 50% aerodynamic cutoff diameter of 1  $\mu\text{m}$ . The airstream was not intentionally dried; instead the temperature increase from outdoors

into the heated building reduced the RH of the incoming airstream.

[13] Aerosol absorption ( $\sigma_{\text{ap}}$ ) at three wavelengths was measured with a Particle Soot Absorption Photometer (PSAP) (Radiance Research, Shoreline, Washington). This device responds to differential light transmission through a glass fiber filter (E70–2075W, Pallflex Products Corp., Putnam, Connecticut) as particles are loaded onto the filter. The absorption measurement was made immediately downstream of the nephelometer, ensuring that the scattering and absorption properties were measured on the identical aerosol.

[14] The raw scattering and absorption data were collected as 20 s averages and then reduced to 1 h averages. Periods of likely snowcat contamination, identified by simultaneous drastic spikes in NO and aerosol absorption, were removed from the raw data prior to averaging. All scattering and absorption coefficients are reported at a wavelength of 550 nm, 273.15 K and 1013.25 hPa.

#### 2.2.2. Calibration, Data Reduction, and Uncertainty

[15] The TSI nephelometer calibration protocol differed slightly between spring 2008 and spring 2009. Instrument noise was periodically measured and traced throughout the spring 2008 campaign using an inline HEPA filter. The filter was put in-line for a minimum of 30 min at approximately two week intervals. No trend was noted in the zero data. Multiple calibrations following the manufacturer's protocol were performed, and we used data from these calibrations to estimate the drift uncertainty following equation (8) of Anderson and Ogren [1998] with the manufacturer's calibration constants. The measured data were corrected for angular nonidealities, which cause particle scattering in the near forward direction to be underestimated.

[16] The TSI nephelometer was serviced and calibrated by the manufacturer just prior to the spring 2009 campaign. During the spring 2009 campaign the TSI nephelometer was periodically switched to measure both particle free air and  $\text{CO}_2$ . The measured values were corrected for offset and calibration drift in addition to angular nonidealities [Anderson and Ogren, 1998]. The filtered air and  $\text{CO}_2$  were measured approximately every two weeks [Anderson and Ogren, 1998]. The data reduction and uncertainty analysis that we followed for the scattering data are outlined by Anderson and Ogren [1998]. Sources of uncertainties associated with the nephelometer include photon counting noise, zeroing and calibration, and the correction for angular nonidealities. Combined these errors yielded a total uncertainty of  $\pm 8\%$  for a scattering coefficient of  $30 \text{ Mm}^{-1}$ , a 60 min averaging time and a wavelength of 550 nm.

[17] The three-wavelength PSAP is a relatively new instrument, and it is a modified version of the single-wavelength PSAP. The single-wavelength PSAP has been calibrated and intercompared with other filter based aerosol absorption techniques [Bond *et al.*, 1999]. A prototype version of the three-wavelength PSAP was calibrated against two other absorption standards in 2002. The goal was to derive loading correction functions and filter/aerosol scattering correction factors for each of the three wavelengths [Sheridan *et al.*, 2005; Virkkula *et al.*, 2005]. A similar study has not been performed with the commercially available model, but the only difference between the commercially available model and that used by Virkkula *et al.* [2005] is in the light source geometry. The prototype used an elliptical grating to par-

**Table 1.** Absorption Data Adjustments and Uncertainties<sup>a</sup>

Source	Correction	Uncertainty (Mm <sup>-1</sup> )	Notes
Flow rate	$\sigma_{\text{PSAP}}^*(F_{\text{PSAP}}/F_{\text{meas}})$	$\delta F_{\text{meas}}^* \sigma_{\text{PSAP}}$	$\delta F_{\text{meas}}$ in this case was 0.01 for a Sensidyne Gilibrator flowmeter
Spot size	User enters the correct spot size for that particular instrument. Instrument calculates correction.	$0.08^* \sigma_{\text{PSAP}}$	4% uncertainty on the measured diameter results in an 8% uncertainty in the spot area, and thus the absorption coefficient [Virkkula <i>et al.</i> , 2005].
Noise	–	0.18 $\sqrt{(\tau_o/\tau)}$ Clean Filter 0.3 $\sqrt{(\tau_a/\tau)}$ Dirty Filter 0.3*5 $\sqrt{(\tau_a/\tau)}$	PSAP noise does not depend on $\sigma_{\text{ap}}$ . $\tau_o$ is 24 min, $\tau$ is 60 min for this study. The first correction factor is the reported noise for the single wavelength PSAP operated at constant altitude [Anderson <i>et al.</i> , 1999]. Anderson <i>et al.</i> [2003] performed duplicate absorption measurements to examine instrumental noise. Noise is larger when the PSAP is exposed to changing altitudes and changing humidity. Noise also increases with filter loading. They found that noise for a clean filter at a constant pressure is 0.3 for a 30 s time resolution ( $\tau_a = 30$ s). Noise for a dirty filter is 5 times higher [Anderson <i>et al.</i> , 2003]. Consistent results were found during a comparison of three three-wavelength PSAPs prior to INTEX-B [McNaughton <i>et al.</i> , 2009].
Drift	–	0.06 $\sigma_{\text{am}}$	Drift corrections cannot be made because calibrations were not made in the field. This value is based on parallel measurement from 3 single wavelength PSAPs [Anderson <i>et al.</i> , 1999]. Anderson <i>et al.</i> [2003] report a 5% systematic discrepancy from 2 single wavelength PSAPs operated in parallel. Similar unpublished tests with the three wavelength PSAPs are consistent.
Calibration	–	0.20* $\sigma_{\text{ap}}$	Bond <i>et al.</i> [1999]
Scattering response	$-S_\lambda^* \sigma_{\text{spm}}$ 467 nm $S_\lambda$ mean(min, max) = 0.012 (0.009, 0.020) 530 nm $S_\lambda$ mean(min, max) = 0.016 (0.011, 0.023) 660 nm $S_\lambda$ mean(min, max) = 0.021 (0.016, 0.029)	0.07* $\sigma_{\text{spm}}$	The scattering response was determined for a prototype model [Virkkula <i>et al.</i> , 2005]. The scattering data are adjusted to PSAP wavelengths. $\sigma_{\text{spm}x} = \sigma_{\text{spm}1}(\lambda_1/\lambda_x)\alpha^{12}$ $\alpha_{12} = -\log(\sigma_{\text{spm}1}/\sigma_{\text{spm}2})/\log(\lambda_1/\lambda_2)$

<sup>a</sup>Applies to data collected with a three-wavelength PSAP. The correction to the PSAP data can be summarized as  $\sigma_{\text{ap}} = \sigma_{\text{PSAP}}^*(F_{\text{PSAP}}/F_{\text{meas}}) - S_\lambda^* \sigma_{\text{spm}}$  (equation (1)). Notation:  $\sigma_{\text{ap}}$ , absorption photometer measurement after flow rate and scattering corrections;  $\sigma_{\text{am}}$ , absorption photometer measurement after flow rate and spot area corrections;  $\sigma_{\text{PSAP}}$ , absorption photometer measurement prior to any corrections;  $\sigma_{\text{spm}}$ , nephelometer measurement after adjustment for measurements of calibration gases;  $F_{\text{PSAP}}$ , PSAP flow as reported by PSAP internal flowmeter;  $F_{\text{meas}}$ , PSAP flow as measured by Sensidyne Gilibrator flowmeter;  $\delta F_{\text{meas}}$ , uncertainty in flow rate measured by Sensidyne Gilibrator flowmeter;  $\tau = 60$  min averaging time.

tially collimate the light from the LEDs into the light path to the filter. The commercial model uses an integrating hemisphere to produce a uniform high-intensity LED light source. The light source illuminates the cylindrical port and sample flow path to the filter holder. The LED wavelengths are the same. There are no significant differences in the rest of the filter and light path geometry of the two instruments. We do not expect significant performance differences between the prototype three-wavelength PSAP used in the Virkkula *et al.* [2005] study and the instruments used at MBO.

[18] Bond *et al.* [1999] present several important observations of the single-wavelength PSAP, all of which are applicable to the three-wavelength version of the PSAP. (1) The flowmeter in the PSAP can be in error by as much as 20%; therefore it is necessary for the operator to periodically measure and record the flow independently with a high-accuracy flowmeter. (2) There is variation in the sample spot size between instruments. The spot size must be measured on each individual instrument. (3) Aerosol loading onto the filter can magnify the absorption and create a nonlinear response in the absorption signal. (4) The PSAP interprets a small amount of aerosol scattering as absorption.

[19] The software in the commercially available three-wavelength PSAP includes a transmission correction function, and this function does an adequate job at low absorption values and at  $\omega$  values above  $\sim 0.80$  [Sheridan *et al.*, 2005; Virkkula *et al.*, 2005]. It also allows the user to enter the correct spot size for that particular instrument. Therefore,

many users only need to apply two corrections when processing the data that is output from the instrument: a flow rate correction and a scattering correction. During the spring 2008 and 2009 campaigns at MBO, the instrument flow was accurately measured on a biweekly basis with a Sensidyne Gilibrator flowmeter (reading accuracy:  $\pm 1\%$ ), and a correction factor was applied as described by Bond *et al.* [1999]. Then the scattering corrections summarized by Virkkula *et al.* [2005] were applied (1.3%, 1.6%, and 2.1% for 467 nm, 530 nm, and 660 nm, respectively). The scattering data used in the corrections (measured with a TSI nephelometer at 450, 550, and 700 nm) were adjusted to the PSAP measurement wavelengths as described by Virkkula *et al.* [2005].

[20] Finally, we assumed a power law relationship between absorption and wavelength so both the absorption and scattering data could be reported at the same wavelengths. The 467–530 nm pair was used to adjust absorption at 467 nm to 450 nm. The 467–660 nm pair was used to adjust absorption at 530 nm to 550 nm. Finally, the 530–660 nm pair was used to adjust absorption at 660 nm to 700 nm. Similar to the single-wavelength PSAP, sources of uncertainty in the three-wavelength PSAP measurement include noise, drift, errors in the loading function, the correction for the scattering artifact, and uncertainty in the flow and spot size corrections [Anderson *et al.*, 2003, 1999; Bond *et al.*, 1999; Virkkula *et al.*, 2005]. Combined these errors yielded a total uncertainty of  $\sim 20\%$ . We have summarized the corrections and the main known sources of uncertainty in the PSAP

measurements in Table 1. The correction to the PSAP data can be summarized as

$$\sigma_{\text{ap}} = \sigma_{\text{PSAP}} * (F_{\text{PSAP}}/F_{\text{meas}}) - S_{\lambda} * \sigma_{\text{spm}} \quad (1)$$

and all variables are defined in Table 1.

[21] It is important to be aware of the correction scheme that is used to correct the PSAP measurements from various campaigns. A full set of calibration factors for the three-wavelength PSAP is provided by *Virkkula et al.* [2005]. At the low  $\omega$  and low filter loadings characteristic of MBO, the absorption coefficients would be  $\sim 30\%$  lower if the Virkkula scheme was used. This would yield the higher  $\omega$  values presented in auxiliary material Table S1.<sup>1</sup> The reasons for the discrepancy are not clear and have been noted by other authors [*Sierau et al.*, 2006]. Previous studies have also not used the full *Virkkula et al.* [2005] correction scheme, and have instead relied on the manufacturer's transmission function as was done here. For example, *Sierau et al.* [2006] chose to adapt the findings of *Bond et al.* [1999] to the three-wavelength absorption data. This choice includes an additional 22% correction than applied here. *McNaughton et al.* [2009] used the full *Virkkula et al.* [2005] correction scheme in processing airborne absorption measurements from INTEX-B. We have processed our data in each way (Table 2 and auxiliary material Table S1), and although the magnitude of  $\omega$  is impacted, the choice of correction scheme does not impact our major findings.

[22] Finally significant consideration should be given to where filter-based absorption measurements are deployed and how they are eventually interpreted. A major drawback to filter based measurements is that the aerosols are deposited onto the filter before the absorption is measured, and this can alter their physical state. This is especially true for liquid-like organic aerosols which can be redistributed around filter fibers, modifying the filter surface and increasing the scattering artifact beyond that accounted for in the *Bond et al.* [1999] and *Virkkula et al.* [2005] corrections [*Subramanian et al.*, 2007]. Liquid-like organic material can also coat any absorbing material already present on the filter and enhance absorption [*Lack et al.*, 2008]. *Lack et al.* [2008] show that the PSAP can overestimate absorption and this bias is dependent on the amount of organic aerosol present. The PSAP has also recently been shown to have a systematic size-dependent bias, and absorption is under reported for the case of coated absorbing spheres [*Lack et al.*, 2009]. Despite these concerns, the PSAP can provide reasonable aerosol absorption measurements in remote regions with relatively low organic mass loadings. MBO fits the requirements of a location where the PSAP provides reasonable measurements.

[23] We present both precision uncertainty and total uncertainty as described by *Anderson et al.* [1999]. Briefly, precision uncertainty includes uncertainty associated with noise and calibration drift. It allows for the comparison of measurements collected using the same instruments and protocols to be statistically compared. This is the appropriate uncertainty to consider when comparing optical properties among the individual Asian aerosol plumes observed at

MBO during this study period. It is also appropriate to use this uncertainty to compare measurements made in other locations with similar instruments and protocols. Total uncertainty includes precision uncertainty, the uncertainty associated with the corrections we applied to the data, and the uncertainty associated with the calibration method. This is the appropriate uncertainty to consider when comparing the measurements presented in this study with optical data collected using other measurement methods. We do not include uncertainty for the sampling efficiency in any of the calculations; this includes aerosol loss in the inlet or sampling line which should be insignificant compared to the other uncertainties for the submicrometer aerosol fraction.

### 2.2.3. Derived Intensive Properties

[24] The scattering and absorption coefficients were converted to the dimensionless intensive optical properties of  $\mathring{A}_s$ ,  $\mathring{A}_a$ ,  $\omega$ , and  $b$  as follows:

$$\mathring{A}_s = -\log(\sigma_{\text{sp}}^{450}/\sigma_{\text{sp}}^{700})/\log(450/700), \quad (2)$$

$$\mathring{A}_a = -\log(\sigma_{\text{ap}}^{450}/\sigma_{\text{ap}}^{700})/\log(450/700), \quad (3)$$

$$\omega = \sigma_{\text{sp}}/(\sigma_{\text{ap}} + \sigma_{\text{sp}}), \quad (4)$$

$$b = \sigma_{\text{bsp}}/\sigma_{\text{sp}}, \quad (5)$$

where  $\omega$ , and  $b$  are referenced to 550 nm wavelength and the superscripts in (2) and (3) refer to the other wavelengths measured by the nephelometer.  $\mathring{A}_s$  was also calculated using the 550 and 700 nm pair to facilitate comparison with previously published measurements. Uncertainties in the intensive properties are calculated from the uncertainties in the extensive properties. The uncertainty is propagated such that the uncertainty in intensive property  $X(y, z)$ ,  $\delta X$ , is given by

$$\delta X = \left\{ [(\delta y) * (\partial X / \partial y)]^2 + [(\delta z) * (\partial X / \partial z)]^2 \right\}^{1/2}, \quad (6)$$

where  $\delta y$  and  $\delta z$  are the uncertainties in the extensive properties  $y$  and  $z$ .

### 2.3. Compositional Analysis of the PSAP Filters

[25] After the filters were removed from the PSAP, trace element analyses were performed by using reflectance X-ray fluorescence (XRF) spectroscopy (S2 Picofox, Bruker Instruments). This instrument uses a molybdenum X-ray tube with Ni/C multilayer grating to generate a monochromatic X-ray excitation beam that is focused on the sample using very low grazing angle (0.3–0.6 degrees). This allows for total reflection of the beam. The fluorescence spectrum is obtained at a 90 degree angle from the sample using an XFlash detector (Bruker, 10 mm<sup>2</sup> area, FWHM: <160 eV @ Mn K $\alpha$  line). The use of reflectance XRF minimizes matrix effects in the aerosol samples without extensive sample pretreatment. Elements from sodium to uranium are accessible with this system with the exception of zirconium, niobium, molyb-

<sup>1</sup>Auxiliary materials are available in the HTML. doi:10.1029/2010JD013943.

**Table 2.** Optical Measurements for Each of the Seven Asian Air Masses Observed at MBO in Spring 2008 and Spring 2009<sup>a</sup>

	$\sigma_{\text{sp}}$ ( $\text{Mm}^{-1}$ )	$\sigma_{\text{ap}}$ ( $\text{Mm}^{-1}$ )	$\omega$	$\tilde{A}_{\text{s}}$	$\tilde{A}_{\text{a}}$	$b$
<i>Plume A: 17 April 2008 1900 GMT to 18 April 2008 1800 GMT<sup>b</sup></i>						
Peak	33.78	5.67	—	—	—	—
Average	16.11	2.53	0.862	2.33	1.30	—
S.D.	8.29	1.33	0.014	0.15	0.11	—
Prec uncer	0.20	0.06	0.004	0.10	0.08	—
Tot uncer	0.29	0.23	0.006	0.11	0.13	—
<i>Plume B: 25 April 2008 1500 GMT to 28 April 2008 2300 GMT<sup>c</sup></i>						
Peak	34.76	4.11	—	—	—	—
Average	19.61	2.57	0.889	1.99	1.38	—
S.D.	5.98	0.75	0.019	0.12	0.08	—
Prec uncer	0.13	0.16	0.007	0.04	0.04	—
Tot uncer	0.21	0.17	0.017	0.05	0.09	—
<i>Plume C: 12 May 2008 1000 GMT to 13 May 2008 1200 GMT<sup>d</sup></i>						
Peak	12.71	1.35	—	—	—	—
Average	9.84	1.17	0.892	2.61	1.41	—
S.D.	1.73	0.14	0.010	0.07	0.08	—
Prec uncer	0.19	0.03	0.013	0.12	0.10	—
Tot uncer	0.24	0.10	0.019	0.14	0.15	—
<i>Plume D: 17 April 2009 0500 to 0800 GMT<sup>e</sup></i>						
Peak	30.80	4.32	—	—	—	—
Average	24.45	3.43	0.875	1.99	1.18	0.115
S.D.	5.05	0.64	0.023	0.06	0.02	0.001
Prec uncer	0.49	0.14	0.005	0.08	0.13	0.008
Tot uncer	1.00	0.38	0.013	0.14	0.35	0.010
<i>Plume E: 18 April 2009 0200 GMT to 19 April 2009 0500 GMT<sup>f</sup></i>						
Peak	20.11	2.73	—	—	—	—
Average	10.48	1.57	0.868	2.22	1.27	0.129
S.D.	4.82	0.66	0.011	0.08	0.05	0.007
Prec uncer	0.23	0.05	0.005	0.09	0.11	0.012
Tot uncer	0.34	0.17	0.008	0.13	0.22	0.013
<i>Plume F: 25 April 2009 0200 to 2300 GMT<sup>g</sup></i>						
Peak	21.33	2.91	—	—	—	—
Average	17.70	2.27	0.886	2.07	1.09	0.117
S.D.	2.28	0.37	0.012	0.04	0.10	0.004
Prec uncer	0.24	0.06	0.003	0.05	0.09	0.006
Tot uncer	0.41	0.24	0.006	0.08	0.19	0.007
<i>Plume G: 15 May 2009 0500 GMT to 16 May 2009 1400 GMT<sup>h</sup></i>						
Peak	14.02	1.23	—	—	—	—
Average	9.34	0.92	0.909	1.78	1.28	0.114
S.D.	1.60	0.16	0.012	0.39	0.26	0.007
Prec uncer	0.16	0.03	0.003	0.06	0.10	0.008
Tot uncer	0.21	0.10	0.005	0.08	0.17	0.009

<sup>a</sup>Data were corrected for the filter spot size, the flow rate and the scattering response as described in section 2.2.2. The averages are based on hourly data, and the uncertainty pertains to the average. Aerosol scattering ( $\sigma_{\text{sp}}$ ) and absorption coefficients ( $\sigma_{\text{ap}}$ ) are at STP and represent submicrometer dry aerosol. The average values exclude data from 1100–1900 Local Time when the local mixed layer may have been influencing MBO. S.D., standard deviation; Prec uncer, precision uncertainty; Tot uncer, total uncertainty.

<sup>b</sup>HYSPLIT trajectories and GEOS—Chem suggest a predominantly biomass burning source near Lake Baikal. Plume travelled over great circle in ~5–6 days.

<sup>c</sup>Satellite images, CALIPSO and IMPROVE data suggest a mixture of dust and smoke, primarily dust. Plume travelled over the great circle in ~7–9 days.

<sup>d</sup>Trajectories passed over NE China and Northern Japan ~7–9 days back from MBO, then over a region of fires near Lake Baikal ~9–10 days back from MBO.

<sup>e</sup>HYSPLIT trajectories pass over Northeastern China and Northern Japan ~7–9 days back from MBO.

<sup>f</sup>HYSPLIT trajectories initialized 19 April 0300–0600 UTC pass through boundary layer in Northeastern China 5 days back from MBO.

denium, and technetium due to their use in the excitation source.

[26] For the XRF analysis, the PSAP filters were fixed to acrylic sampling discs using a thin layer of silicon grease (Dow Corning® 7 Release Compound) and placed into a sample tray. These discs were inserted into the XRF instrument with the sample side facing the X-ray excitation beam. Blank filters were handled and analyzed in the same manner as the samples, and the blank concentration levels were subtracted from the sample concentrations. For this analysis, the elemental concentrations were determined using argon as an internal standard. The quantification was performed automatically by the Picofox Software using the concentration of this internal standard, the net pulse number, and the relative sensitivity of both argon and the element to be analyzed within the measurement spectrum. The detection limits are based on the three-sigma criterion.

[27] The composition information derived from the PSAP filters was only used qualitatively in our analysis to support other sources of information on aerosol composition. Isolating the elemental concentrations for the specific plumes presented here is not possible because the PSAP filters were changed on irregular time intervals. Many filters were collected over several day periods, which often included both plume and nonplume conditions. The elemental information was most useful when filter changes coincided closely with plume boundaries, which occurred once on 17–18 April 2008. Unlike for the absorption measurements, we were not able to correct these filter measurements for snow cat contamination. However, these filters represent the only in situ measurements of aerosol chemical composition, so we have chosen to include them here.

## 2.4. Description of Backward Trajectories

[28] We calculated two sets of backward trajectories to establish the transport history of the aerosol plumes. The first set included 10 day back trajectories initialized each hour from the summit of MBO using the Hybrid Single-Particle Lagrangian Integrated Trajectory (HYSPPLIT-4) model (R. R. Draxler and G. D. Rolph, 2003, <http://www.arl.noaa.gov/ready/hysplit4.html>). These 10 day trajectories were calculated using global meteorological data from the GDAS (Global Data Assimilation System) archive, which has a time resolution of 3 h, a spatial resolution of 1 degree latitude by 1 degree longitude, and a vertical resolution of 23 pressure surfaces between 1000 and 20 hPa. Trajectories were run at multiple heights surrounding the summit of MBO as in work by Weiss-Penzias *et al.* [2006].

[29] The second set of backward HYSPLIT trajectories were run for 3 days using meteorological data from the EDAS (Eta Data Assimilation System) archive. The EDAS archive grid covers the continental United States after 2004, has a horizontal resolution of 40 km and a vertical resolution of 26 pressure surfaces between 1000 and 50 hPa. These tra-

### Notes to Table 2:

<sup>g</sup>HYSPLIT trajectories show air passed through BL in a region of intense agricultural fires in southwest Russia ~8–10 days back from MBO. Plume travelled over the great circle.

<sup>h</sup>NAAPS indicates the presence of dust over the Pacific Northwest. HYSPLIT trajectories show air mass passed through NE China ~10 days prior to reaching MBO.

jectories were initialized from 1200 m above model ground level for each hour of the spring campaign. The trajectories were initialized above the ground since both the GDAS and the EDAS model define the terrain for the grid box containing MBO significantly below the actual altitude of Mount Bachelor. Error in HYSPLIT trajectory calculations normal to the direction of flow are 10–30% of the distance traveled after 24 h [Draxler and Hess, 1998].

## 2.5. Other Supporting Measurement Networks and Platforms

[30] We considered several ground based networks, satellite platforms, and model output as supporting data in our analysis of individual aerosol plumes. Supporting data are described here, and it was only included in our analysis if it coincided with observations at MBO. Thus different data sets were explored for each aerosol plume as needed. We do not attempt a quantitative comparison with the supporting data sets, and they are primarily used as a source of qualitative information on the chemical composition of the aerosols observed at MBO.

[31] IMPROVE monitoring sites are situated in National Parks and Class I Wilderness Areas across the United States (<http://vista.cira.colostate.edu/improve/>). Speciated fine aerosol ( $<2.5 \mu\text{m}$ ),  $\text{PM}_{2.5}$  mass and  $\text{PM}_{10}$  mass are measured at all IMPROVE sites. Samples are collected every three days [Malm *et al.*, 1994]. We used aerosol chemical speciation data from the two IMPROVE sites located nearest to MBO (Figure 1): Mount Hood ( $45.288^\circ\text{N}$ ,  $121.7837^\circ\text{W}$ , 1531 m amsl) and Three Sisters Wilderness Area ( $44.291^\circ\text{N}$ ,  $122.0434^\circ\text{W}$ , 885 m amsl).

[32] Data from the Cloud-Aerosol Lidar and Infrared Pathfinder Satellite Observation (CALIPSO) [Liu *et al.*, 2009] were used to corroborate plume height and type when an overpass coincided with a period of interest at MBO and an aerosol plume was clearly defined in the CALIPSO data swath. CALIPSO uses the layer integrated attenuated backscatter, the volume depolarization ratio, surface type and elevation to determine aerosol type [Omar *et al.*, 2009]. The six aerosol types (clean continental, clean marine, dust, polluted continental, polluted dust, and smoke) are representative of aerosol mixtures most frequently observed at AERONET sites (AEROSOL ROBOTIC NETWORK, <http://aeronet.gsfc.nasa.gov/>) [Omar *et al.*, 2005]. CALIPSO orbits in the “A-Train” satellite constellation which includes the Aqua, CloudSat, CALIPSO, PARASOL, and the Aura satellite missions.

[33] The Naval Research Laboratory Aerosol Analysis and Prediction System (NAAPS, <http://www.nrlmry.navy.mil/aerosol/>) uses real-time satellite observations to forecast the distribution of tropospheric aerosols resulting from biomass burning, dust storms, and anthropogenic  $\text{SO}_2$  emissions. These forecasts have been archived since 2000 are readily available on line. The NAAPS simulations are useful because they use operational dynamics, are operated in real time, and provide simulations with global coverage. Keeping in mind the constraints on the input (satellite estimates of smoke and dust), the NAAPS output provides one of the only opportunities to continuously identify periods and geographic regions potentially impacted by pollution, biomass burning smoke or dust plumes. Similar to several previous studies, we used NAAPS forecasts qualitatively to identify regions and time periods potentially impacted by upwind

aerosol source regions [Jaffe *et al.*, 2004; Lapina *et al.*, 2006; Morris *et al.*, 2006].

## 3. Results

### 3.1. Identification of Asian Pollution Episodes

[34] Presented here is a general overview of the MBO aerosol data, and how the Asian aerosol plumes were identified. Figure 2 presents a time series of hourly averaged  $1 \mu\text{m}$   $\sigma_{\text{sp}}$  and  $\sigma_{\text{ap}}$  measured at MBO during spring 2008 and 2009. The seven Asian aerosol plumes are highlighted in Figure 2. We used the HYSPLIT trajectories calculated using the global GDAS meteorological grid to define periods of likely Asian influence. In each case, the air mass impacting MBO descended during the final 24 h of transport to the site as confirmed by the HYSPLIT back trajectories calculated using the 40 km EDAS meteorological grid. Local minimums in water vapor (WV) mixing ratio were also observed at MBO simultaneous with the peaks in aerosol scattering. The air mass may have traveled through the lower troposphere over the Pacific en route to North America, but interaction with the North American boundary layer was unlikely. There were other periods during each measurement campaign where the backward trajectories indicated rapid transport from East Asia. However, because the aerosol and gas-phase ( $\text{CO}$ ,  $\text{O}_3$ , PAN) observations showed minimal enhancements or there was not an aerosol plume distinguishable from the relatively low background observations, we chose not to focus on these periods. Instead we focused on the seven highlighted plumes because they clearly showed an enhanced aerosol load, and were often also accompanied by enhancements in gas-phase species. Note that the defined plumes include many of the highest peaks in aerosol scattering and absorption observed at MBO.

[35] Table 2 presents the aerosol optical measurements for each of the Asian air masses based on the hourly averaged data. The data in Table 2 exclude data from 1100–1900 Local Time when the afternoon upslope mountain flow may have caused the local mixed layer to reach the summit of Mount Bachelor [Reidmiller *et al.*, 2010; Weiss-Penzias *et al.*, 2006]. This conservative choice reduces the amount of data included in the statistics, but it ensures that we do not include aerosol with a local source in our analysis. This choice does not change the main conclusions of our analysis.

[36] Of interest in this analysis is (1) whether the intensive optical properties differ between these seven Asian plumes, (2) whether these differences can be linked to differences in chemical composition or source region, and (3) whether the intensive optical properties differ from those measured during previous campaigns using similar instruments closer to the Asian source region.

### 3.2. Plume A: 17–18 April 2008

[37] Elevated  $\sigma_{\text{sp}}$ ,  $\sigma_{\text{ap}}$ ,  $\text{CO}$ ,  $\text{O}_3$ , and PAN mixing ratios were observed from 17 April 1300 GMT to 18 April 1900 GMT (Figure 3a). For example, observed hourly averaged  $\text{CO}$  at MBO reached 195 ppbv; the monthly mean  $\text{CO}$  for April 2008 was 138 ppbv. This plume has been described in detail by Fischer *et al.* [2010], and they concluded that it had a Siberian biomass burning source. Figure 3 presents a time series of the measured and calculated aerosol optical properties for this plume and the other plumes discussed

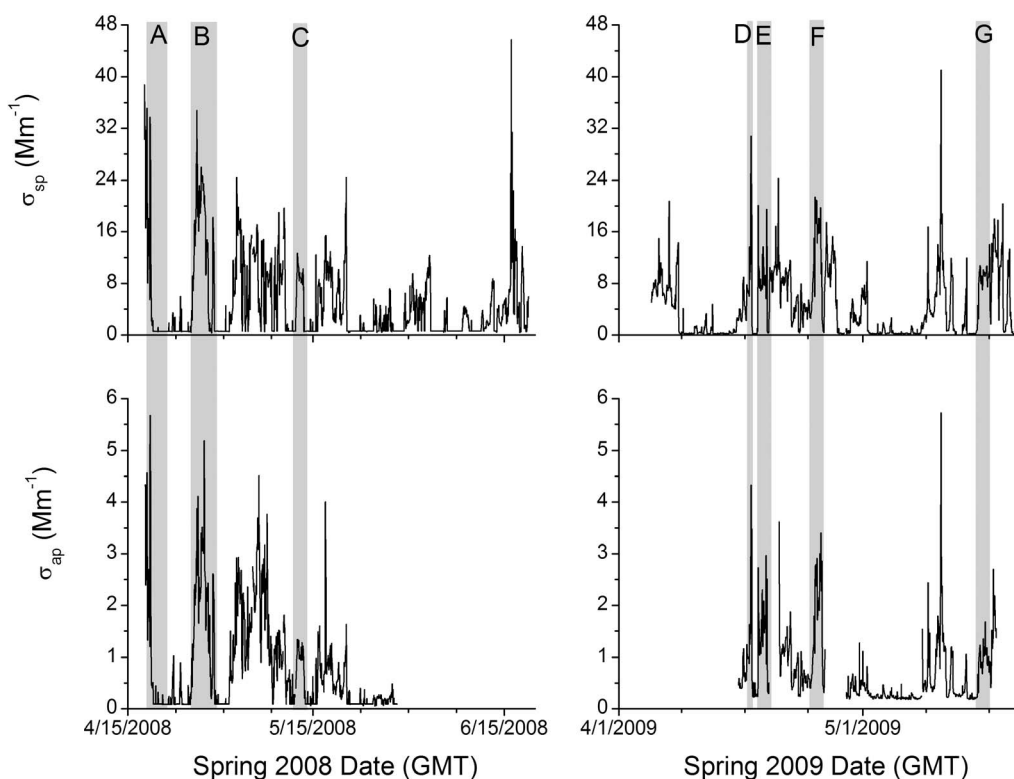


**Figure 2.** Time series of hourly averaged (top) submicrometer aerosol scattering ( $\sigma_{sp}$ ) and (bottom) absorption coefficients ( $\sigma_{ap}$ ) at 550 nm measured at Mount Bachelor during (left) spring 2008 and (right) spring 2009. The gray vertical bars show the time boundaries of the 7 Asian aerosol plumes discussed in this paper.

in sections 3.3–3.8. Biomass burning tracers were also enhanced on the PSAP filters during this time (see auxiliary material Figure S1) [Echalar *et al.*, 1995; Gaudichet *et al.*, 1995; Viana *et al.*, 2008].

[38] The 10 day HYSPLIT back trajectories indicate that transpacific transport was relatively efficient; the plume crossed the Pacific Rim in approximately 5 days. Prior to reaching MBO, the trajectories passed through a region of active fires in southeastern Russia near Lake Baikal and the Chinese border. A global chemical transport model (GEOS-Chem) simulated the timing and magnitude of the observed PAN and CO well, and the model supports a Siberian biomass burning source for these aerosols [Fischer *et al.*, 2010]. The air mass containing the aerosol plume arrived at MBO from the northwest under strongly subsiding conditions during a period of cold air advection over the Pacific Northwest.

### 3.3. Plume B: 25–28 April 2008

[39] Although interpretation of the HYSPLIT back trajectories during this period is not straightforward, there is strong evidence that this aerosol plume was a mix of dust and smoke from Asia. Aerosol scattering and absorption began to rise at MBO late on 25 April 2008 and remained above  $15 \text{ Mm}^{-1}$  for 48 h (Figure 3b). This was the longest period of elevated  $\sigma_{sp}$  observed at MBO during spring 2008. After a 12 h period where  $\sigma_{sp}$  was below detection limit, MBO intercepted a second plume with similar intensive optical

properties for 5 h on 28 April 2008. The peak in  $\sigma_{sp}$  and  $\sigma_{ap}$  was observed at ~0400 GMT on 26 April 2008. This hourly averaged peak was accompanied by 140 ppbv CO; CO reached 171 ppbv later on 26 April. Averaged over the duration of this plume, both CO and  $\text{O}_3$  were lower during this plume than they were for either of the other Asian plumes (A and C) we observed during spring 2008, consistent with dust as a main aerosol type [Price *et al.*, 2004]. This plume had a low average  $\text{\AA}_s$ , indicating a larger aerosol size distribution within the submicrometer portion of the aerosol (Table 2).

[40] Aerosols were also enhanced at lower elevation surface sites across WA and OR coincident with the elevated  $\sigma_{sp}$  and  $\sigma_{ap}$  at MBO. Figure 4b presents a time series of  $\text{PM}_{2.5}$  (by nephelometer) observed in Bend, OR (1100 m amsl). The Bend data show pronounced daily afternoon peaks in aerosol concentration, which support entrainment of aerosol into the BL from above. The dashed lines in Figure 4b surround the same time period that is displayed in the MBO time series presented in Figure 4a (and Figure 3b). It is interesting to note the period of elevated  $\text{PM}_{2.5}$  centered on 18 April coincident with Plume A. Unlike Plume B, during Plume A coincident elevated  $\text{PM}_{2.5}$  was observed only at some stations in OR and not in WA. The scale of Plume B, observed at widely separated sites, argues against a local aerosol source.

[41] Nearby IMPROVE aerosol data provide evidence supporting a dust and smoke source; however, the samples

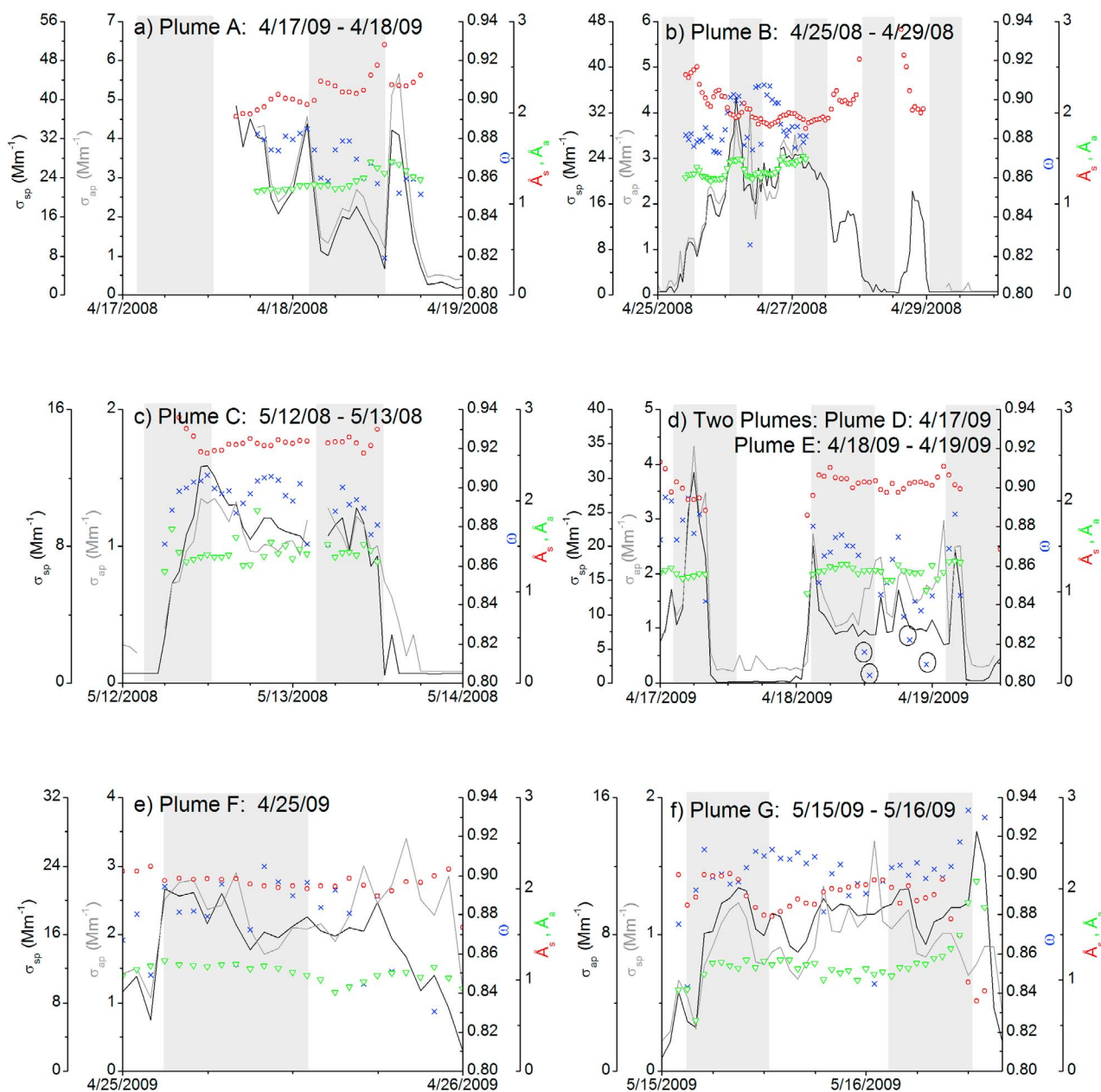


**Figure 3.** Time series of measured and calculated aerosol optical properties at MBO for the seven plumes highlighted in Figure 2. The black line is  $\sigma_{sp}$  at 550 nm and STP. The gray line is  $\sigma_{ap}$  at 550 nm and STP. Hourly averaged  $\omega$  at 550 nm,  $\hat{A}_s$ , and  $\hat{A}_a$  are plotted as blue crosses, red circles, and green triangles, respectively. All time is in GMT. Note that the  $\sigma_{sp}$  and  $\sigma_{ap}$  scales vary but are always set to an 8:1 ratio. Therefore overlaying lines indicate  $\omega = 8/9 = 0.89$ . Two plumes are presented in Figure 3d, where we have circled the points where there was likely local snowcat contamination. In all subplots, the intensive variables were not calculated when either  $\sigma_{sp}$  or  $\sigma_{ap}$  were below detection limit. The light gray shading indicates local sunset to sunrise.

were collected over a period of 24 h and may contain some aerosol not associated with the Asian plume. Figures 4c and 4d present IMPROVE  $PM_{2.5}$  speciation data from the Three Sisters (THIS) monitoring site (see Figure 1 for location). Again, the dashed lines in Figures 4c and 4d surround the same time period that is displayed in the MBO time series presented in Figure 4a. There was one IMPROVE sample on 27 April 2008 that is relevant to this discussion,

but we show the period from 15 March to 15 May for context. The THIS sample on 27 April had the highest fine ( $PM_{2.5}$ ) elemental carbon (EC), organic carbon (OC) and potassium (K) for this period. Figure 4d presents IMPROVE fine soil and sulfate; both of these constituents were also elevated on 27 April. A time series for the Mount Hood (MOHO) IMPROVE site revealed similar patterns in these constituents. We calculated the elemental ratios between the

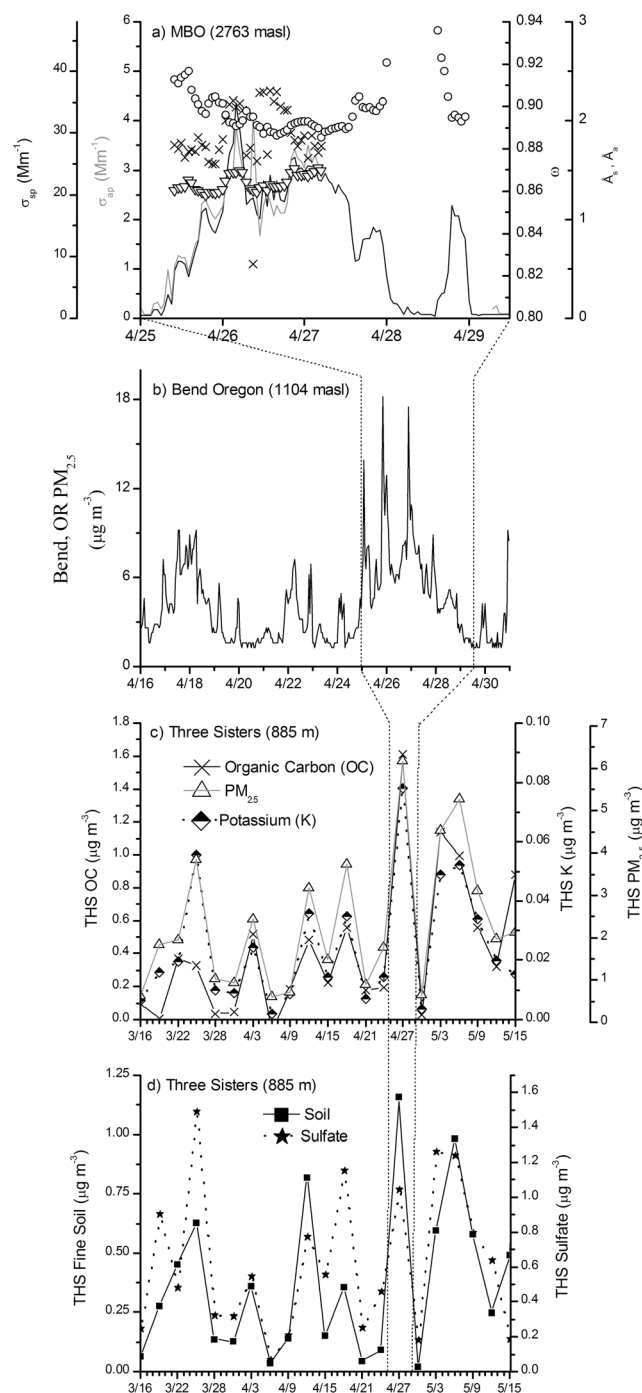


**Figure 4.** (a) Time series of observed and calculated sub-micrometer aerosol optical properties at MBO for the period 25 April 2008 0400 GMT to 29 April 2008 0400 GMT (Plume B). As in Figure 3, Hourly averaged  $\omega$  at 550 nm,  $\hat{A}_s$ , and  $\hat{A}_a$  are plotted as crosses, circles, and triangles, respectively. (b) Time series of  $PM_{2.5}$  observed at Bend, Oregon, for the second half of April 2008. (c) Time series of IMPROVE fine ( $PM_{2.5}$ ) organic carbon (OC),  $PM_{2.5}$  mass, and potassium (K) for the Three Sisters monitoring site (44.29°N, 122.043°W, 885 m), and (d) Time series of IMPROVE fine soil and sulfate for the Three Sisters monitoring site. The dashed lines in Figures 4b, 4c, and 4d surround the same time period that is displayed in Figure 4a).

major IMPROVE soil constituents (Fe, Al, Si, Ca, Ti) and K for the 27 April samples at the THIS and MOHO sites. A least squares linear regression between the THIS and MOHO daily elemental ratios yielded a slope of 0.97 and a  $R^2 = 0.99$ , which indicates a common source [DeBell *et al.*, 2004].

[42] The CALISPO classification for Plume B corroborates the IMPROVE data. There were two relevant CALISPO overpasses that we considered. The first occurred on 25 April 2008 and identified a dust layer of aerosol off the British Columbia and Washington coast (auxiliary material Figure S2). The second CALISPO overpass occurred on 27 April and the swath was almost directly over MBO where an aerosol layer near the surface was visible. This layer was classified as a mixture of dust (~37%) and polluted dust (~63%).

[43] The 10 day HYSPLIT backward trajectories associated with this time period were difficult to interpret owing to a strong low-pressure system situated in the Gulf of Alaska. Most of the backward trajectories circled around the Gulf of Alaska, never reaching Asia. The 3-day HYSPLIT backward trajectories calculated using the EDAS grid show rapid descent from the northwest in the 2 days prior to MBO for 26 April. These trajectories show a shift to a southern approach from within the continental boundary layer on April 27, corresponding to the drop in aerosol scattering at MBO. Because the 10 day backward trajectories were unreliable due to the strong cyclone, we used a variety of supporting satellite data and model output to establish the long-range transport history of the air mass impacting MBO.

[44] NAAPS images (not shown) indicate elevated surface concentrations of smoke and dust in the Lake Baikal and Gobi desert regions on 17–18 April. The plume can be seen in visible images over this region at this time, and crossing the Kamchatka Peninsula 2 days later. A period of elevated aerosol load centered on 21 April was observed at the surface in Anchorage, Fairbanks, and Juneau, Alaska. Several CALISPO swaths identify a deep (~5 km) layer of aerosol over Alaska coincident with these surface measurements. It is unclear whether the majority of the plume traveled south over the Gulf of Alaska or over interior BC. At least a portion of the plume can be seen in MODIS and MISR images approaching the Washington and Oregon coast on 24 and 25 April (auxiliary material Figure S2). On the basis of these various data sources, we hypothesize that the majority of the plume traveled to MBO over the Pacific Rim and not over interior British Columbia.

### 3.4. Plume C: 12–13 May 2008

[45] Here we focus our attention on the last distinct Asian aerosol plume observed during the spring 2008 campaign. Similar to Plume A, the observed gas-phase species in this plume have been described in detail by Fischer *et al.* [2010] so only a brief summary will be presented here. Carbon monoxide,  $O_3$  and PAN mixing ratios rose throughout 11 May, with a sharp rise in  $\sigma_{sp}$  and  $\sigma_{ap}$  observed on 12 May (Figure 3c). The plume ended abruptly 13 May 1200 GMT. The hourly averaged CO reached 168 ppbv; the average CO mixing ratio observed at MBO during May 2008 was 127 ppbv. The small standard deviations reported in Table 2 and Figures 6, 8, and 9 reflect that the extensive and intensive aerosol optical properties were very consistent

throughout this plume. This plume had the largest average  $\text{\AA}_s$ , indicating that this was the smallest size distribution that we observed in the Asian plumes. In contrast to the previous two plumes we have discussed thus far, this plume took a more southerly route straight across the Pacific. Some of the 10 day backward trajectories passed through industrialized regions of East Asia, while many actually passed north of the major industrialized regions of China, and through a region of southeastern Russia and northeastern China impacted by biomass burning. The source of these aerosols was likely a mixture of biomass burning and industrial pollution. The plume descended strongly under high pressure in the 48 h prior to reaching MBO.

### 3.5. Plume D: 17 April 2009

[46] Plumes D and E were observed very close in time, so they could have the same source. We decided to consider these two plumes separately because the rapid drop in  $\sigma_{sp}$  at  $\sim 1000$  GMT 17 April was not due to local scavenging. It was accompanied by a simultaneous drop in CO, PAN and  $\text{O}_3$  indicating a larger air mass change.

[47] CO, PAN and  $\sigma_{sp}$  were elevated throughout the day on 16 April. A brief simultaneous 3 h peak in these species was observed overnight (auxiliary material Figure S3). Coincident WV mixing ratios at MBO were low ( $\sim 1.5$  g/kg). Three day backward HYSPLIT trajectories initialized from MBO at the time of the maximum  $\sigma_{sp}$  (not shown) show that the air mass descended from the southwest over the previous 24 h. The 10 day backward HYSPLIT trajectories suggest that the air mass crossed the Pacific Ocean in approximately 9 days via the Gulf of Alaska.

### 3.6. Plume E: 18–19 April 2009

[48] A 22 h period of elevated  $\sigma_{sp}$  and  $\sigma_{ap}$  was observed from 18–19 April at MBO. The plume was bounded by  $\sim 20 \text{ Mm}^{-1}$  peaks in  $\sigma_{sp}$  (Figure 3d) simultaneous with low WV mixing ratios. The initial spike in  $\sigma_{sp}$  (0300 GMT 18 April) was accompanied by 174 ppbv CO, 70 ppbv  $\text{O}_3$  and 534 pptv PAN. The backward trajectories initialized from MBO at the time of the initial  $\sigma_{sp}$  spike (not shown) suggest that the air mass left southeast Russia and northeast China approximately 7 days before arriving at MBO. Some of the trajectories show looping in the Gulf of Alaska. The final spike in  $\sigma_{sp}$  (0400 GMT 19 April 2009) was accompanied by 153 ppbv CO, 70 ppbv  $\text{O}_3$  and 465 pptv PAN. The trajectories initialized from MBO at the time of the final  $\sigma_{sp}$  spike (auxiliary material Figure S4) suggest rapid transpacific transport from northeast China approximately 5 days prior.

[49] There is strong evidence that aerosols with a non-Asian source were likely also observed during Plume E. There was an increase in WV and T accompanied by a drop in  $\text{O}_3$  during the local afternoon hours of 18 April, possibly indicating the local BL reached the summit. There is a corresponding drop in  $\omega$  during this time as well. Periods of likely local snow cat contamination were noted in the raw data sporadically during 1200–1300 GMT 18 April, and these points are circled in Figure 3d. We do attempt to remove all data that are impacted by local snow cat emissions, but positively identifying this type of contamination can be difficult. These points are plotted in Figure 3d, but were not included in Table 2 or in the summary Figures 6–9 presented in section 4.

### 3.7. Plume F: 25 April 2009

[50] The trajectories suggest that the source of these aerosols may have been agricultural fires in western Russia, primarily located south of Moscow (auxiliary material Figure S5). The aerosols were accompanied by elevated PAN and CO, and by very low WV mixing ratios ( $< 1$  g/kg). The trajectories suggest that the plume traveled over the great circle to MBO and the transport time from western Russia to MBO was 9–10 days.

### 3.8. Plume G: 15–16 May 2009

[51] Figure 3f presents a 36 h period of elevated submicrometer aerosols observed at MBO on 15–16 May 2009. There is strong evidence that this aerosol plume had a large dust component. The 10 day backward trajectories (not shown) indicate that the air mass observed during this time traveled across the Pacific via the great circle. The air mass was lofted out of the Asian boundary layer over eastern Mongolia. The travel time from northeastern China to the U.S. Pacific Northwest was 7–9 days. High  $\text{O}_3$  (up to 94 ppbv hourly average) was observed during the first several hours of the plume; PAN and CO mixing ratios were also elevated although  $\text{O}_3$  was the most extreme. Auxiliary material Figure S6 presents the NAAPS model predicted AOD for the region at 1800 GMT 15 April 2009. A wide band of dust can be seen impacting the Pacific Northwest and continuing further east. CALIPSO passed almost directly over MBO at  $\sim 1000$  GMT 16 April 2009. A band of aerosol, which CALIPSO classified as dust, can be seen extending from  $50^\circ\text{N}$  to  $28^\circ\text{S}$ . In the region near MBO, CALIPSO indicates the aerosol layer extended from approximately 1–3.5 km amsl.

## 4. Optical Properties of Asian Plumes

[52] Scatterplots of the relationship between the intensive aerosol optical properties are presented in Figure 5. The plumes clustered in terms of their scattering and absorption Ångström exponents, indicating a range of sizes and materials present (Figure 5a). Plumes where mineral dust likely made a larger contribution to extinction (Plume B and G) had the lowest  $\text{\AA}_s$ , which suggests that the tail of the coarse mode aerosol extends below  $1 \mu\text{m}$ . The MBO  $\text{\AA}_s$  distributions during Plume B and G indicate that dust aerosol has a detectable influence on the observed submicrometer aerosol optical properties. Plume C stands apart from the other plumes, exhibiting the highest  $\text{\AA}_s$ ; based on backward trajectory calculations, this plume had one of the longest travel times across Pacific. There is also some evidence that portions of this plume descended over the mid-Pacific possibly interacting with the marine boundary layer and precipitation. Both of these factors suggest activation and scavenging of the larger aerosol particles.

[53] Using a plot analogous to Figure 5a, Clarke *et al.* [2007] showed that biomass burning smoke, pollution and dust aerosols observed over North America could be stratified by their combined spectral scattering and absorption properties for the total aerosol sample. The optical measurements presented by Clarke *et al.* [2007] were accompanied by chemical measurements which confirmed the source apportioning. A similar analysis was performed by Yang *et al.* [2009] on aerosol plumes observed in Beijing,

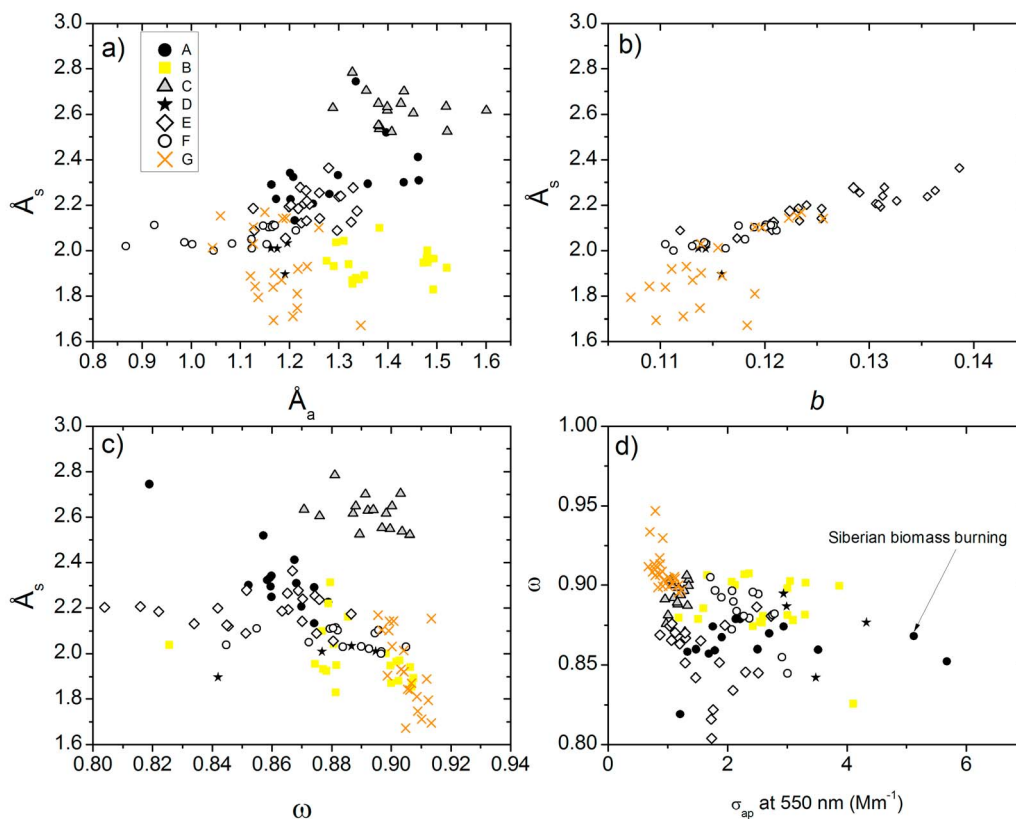


**Figure 5.** (a–c) Scatterplots of the intensive aerosol optical properties of each Asian air mass. Ångström exponents were calculated using the 450–700 nm pair. Backscatter fraction ( $b$ ) and single scatter albedo ( $\omega$ ) are at 550 nm. (d) Single scatter albedo versus absorption. None of these plots include data from 1100–1900 Local Time when the local mixed layer may have been influencing MBO. There is strong evidence that dust made a large contribution to the aerosol scattering in plumes B and G, and Siberian biomass burning smoke made a large contribution to plume A.

and again dust plumes were easily identified by lower  $\tilde{A}_s$  distributions (mean  $\tilde{A}_s = 1.72$  for submicrometer aerosols). In addition to size differences, dust aerosols can also have enhanced absorption at short wavelengths [Patterson, 1981] and thus plumes containing mineral dust can have a higher total aerosol  $\tilde{A}_a$  than plumes primarily composed of biomass burning smoke or anthropogenic pollution [Bergstrom et al., 2007]. Figure 5a suggests that spectral signatures may offer a way to differentiate aerosol plumes observed at MBO without in situ measurements of chemical composition. We hypothesize that this approach would be more useful if it was extended from the submicrometer to the full aerosol size distribution.

[54] There was a positive relationship between  $b$  and  $\tilde{A}_s$ ;  $b$  was larger for smaller particles (Figure 5b). The spring 2009 dust plume (G) had the lowest  $b$ . Model calculations suggest that the scattering phase function of sharp and irregularly shaped particles, such as dust, is larger than those of spherical particles at forward scattering angles ( $\theta < 10^\circ$ ) and smaller at backscattering angles ( $\theta > 150^\circ$ ) [Kalashnikova and Sokolik, 2002]. The observations of  $b$  at MBO are broadly consistent with these modeling results.

[55] Hourly averaged  $\omega$  ranged from 0.83 to 0.93 within the aged Asian plumes (Figures 5c and 5d). Plume C and the plumes hypothesized to contain large amounts of dust

(B and G) had the highest  $\omega$  values. See auxiliary material Table S1 for MBO  $\omega$  values calculated with several PSAP correction schemes.

[56] There is a relatively large amount of variability in  $\omega$  compared to the variability in  $\tilde{A}_s$ . There are several points to note when interpreting Figure 5c: (1) The PSAP has more uncertainty than the TSI nephelometer, so we would expect more variability in the intensive properties calculated using the PSAP absorption measurements. (2) The variability in  $\tilde{A}_s$  is somewhat constrained by the imposed  $1 \mu\text{m}$  size cutoff. (3) Plumes can be layered, and contain several types of aerosols with different scattering to absorption ratios. CALIPSO provides strong satellite evidence that plume B contained layers of dust and smoke. Yang et al. [2009] observed a similar standard deviation in their  $\omega$  measurements of polluted submicrometer dust.

[57] Figure 5d is a plot of  $\omega$  versus absolute absorption at 550 nm. Clarke et al. [2007] used a similar plot (Figure 9a) along with measurements of the size distribution to show that they observed a larger absorption to scattering ratio for smaller particles. Although direct measurements of the aerosol size distribution were not made at MBO, the plumes with a larger size distribution based on their  $\tilde{A}_s$  distributions do exhibit a higher range of  $\omega$  values. This is qualitatively consistent with the Clarke et al. [2007] analysis. Following

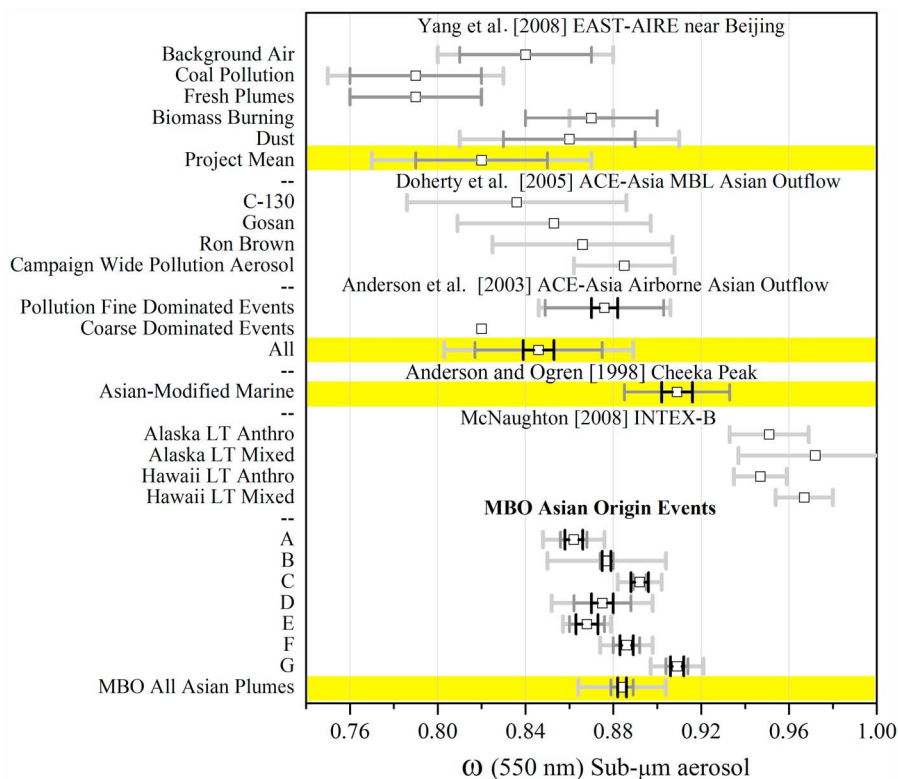


**Figure 6.** Comparison of single scatter albedo ( $\omega$ ) during Asian Origin aerosol plumes measured at MBO during spring 2008 and spring 2009 with other data sets. All values are reported at 550 nm. Light gray, dark gray, and black bars are 1 standard deviation, the total uncertainty of the average, and the precision uncertainty of the average, respectively. This plot does not include data from 1100–1900 Local Time when the local mixed layer may have been influencing MBO. The classifications for the *McNaughton* [2008] data are presented by *McNaughton et al.* [2009]. Briefly, “LT Mixed” represents a mixture of pollution and dust observed in the lower troposphere, and “LT Anthro” represents fine mode dominated aerosol observed in the lower troposphere. The PSAP data from *McNaughton* [2008] were corrected following the full *Virkkula et al.* [2005] correction scheme. See auxiliary material Table S1 for  $\omega$  values calculated for MBO using this correction scheme.

from the analysis of *Clarke et al.* [2007] we expect Plume E to have a smaller size distribution compared to the other plumes. Plume C is possibly inconsistent with the *Clarke et al.* [2007] analysis. Plume C, which likely contains the smallest size distribution based on its  $\dot{A}_s$ , also has a relatively high scattering to absorption ratio.

[58] *Clarke et al.* [2007] also observed a horizontal spread in absorption for the biomass burning plume they encountered, and they concluded that  $\sigma_{sp}$  and  $\sigma_{ap}$  scale together in biomass burning plumes. A similar pattern is evident in plume A, which likely has a Siberian biomass burning source. However, we observed a much smaller range of  $\sigma_{ap}$ .

[59] The optical properties presented here were measured on low-RH submicrometer aerosol. Differences in the observed optical properties reflect variations in aerosol composition rather than humidity. To gain information on how the optical properties of Asian aerosols change when they cross the Pacific, we compare observations of the intensive optical properties at MBO with observations closer to the Asian coast. The comparison is with literature observations of intensive aerosol properties which were not made in the same years as the MBO measurements. Interannual

variability is a major issue, but our main conclusions appear to be robust across different years of measurements made on either side of the Pacific Ocean.

[60] Figures 6–10 are not intended to be Lagrangian studies of the changing optical properties of aerosols within individual plumes. Scarcity of cloud-free satellite data and the difficulty of tracking individual plumes across the Pacific prevent this type of approach. Rather, our goal is to identify patterns in how aerosol modification during transport changes the average intensive aerosol optical properties. We restrict the comparison to data collected using similar instrument configurations during spring months. This type of comparison is inherently difficult, and this type of analysis would certainly be served by additional data.

[61] *Doherty et al.* [2005] present a comparison of the aerosol optical properties measured from multiple platforms during the spring 2001 ACE-Asia field campaign [*Doherty et al.*, 2005; *Huebert et al.*, 2003]. Scattering and absorption were universally measured with TSI integrating nephelometers and single-wavelength PSAPs, respectively. We compare the observations from MBO with observation of Asian outflow made both in the FT [*Anderson et al.*, 2003]

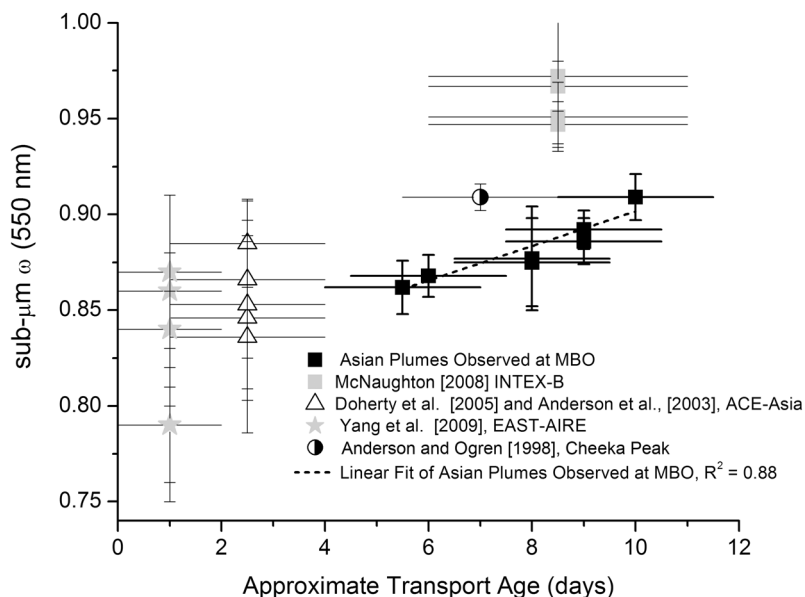


**Figure 7.** Summary plot for single scatter albedo ( $\omega$ ) during Asian origin aerosol plumes measured at MBO during spring 2008 and spring 2009 with the same data sets presented in Figure 6. Here  $\omega$  is plotted as a function of processing time or atmospheric transport age. See text in section 4.1 for a detailed description of how transport age was assessed for each data set. Note the positive relationship between transport time and  $\omega$ . This relationship also holds for plumes observed at MBO, and the linear fit shown here was calculated using only plumes observed at MBO. We remind readers that *McNaughton et al.* [2009] used the full *Virkkula et al.* [2005] correction scheme in processing airborne absorption measurements from INTEX-B. See section 2.2.2 for a discussion of PSAP correction schemes. We have processed our data using several correction schemes (auxiliary material Table S1). When processed using the *Virkkula et al.* [2005] scheme, the resulting  $\omega$  values are larger, closer to those reported by *McNaughton et al.* [2009].

and within the marine BL [*Carrico et al.*, 2003; *Quinn et al.*, 2004]. The scattering and absorption data collected from the cruise are presented by *Quinn et al.* [2004] and were made at a constant RH ( $\sim 55\%$ ), but the data are presented by *Doherty et al.* [2005] at low RH ( $\sim 30\%$ ). The observations presented by *Doherty et al.* [2005] from the marine BL represent several aerosol classes: pollution, marine, dust and volcanic [*Carrico et al.*, 2003]. The full set of aircraft observations, presented by *Anderson et al.* [2003], were separately classified by their sources and the relative contributions of the fine and coarse modes to aerosol scattering.

[62] Aerosol light scattering and absorption were also measured more recently near Beijing as part of the EAST-AIRE (East Asian Study of Tropospheric Aerosols: an International Regional Experiment) campaign during March 2005 [*Yang et al.*, 2009]. *Yang et al.* [2009] segregated the data into air masses dominated by dust, biomass burning, “fresh chimney plumes,” other coal burning pollution, and relatively clean background air for Northern China.

[63] Finally, we also include previous measurements from the eastern Pacific region. The first set of observations of  $\sigma_{sp}$  and  $\sigma_{ap}$  is from Cheeka Peak [*Anderson et al.*, 1999], a coastal low elevation site in northwest Washington that occasionally sees Asian plumes. We have included data from this site during a period impacted by a plume of Asian origin. The second set of observations was from aircraft flights during the Photochemical Ozone Budget of the Eastern North Pacific Atmosphere (PHOBEA) research campaign

[*Jaffe et al.*, 2003b]. The most recent aircraft observations were made during spring 2006 as part of Phase B of the Intercontinental Chemical Transport Experiment (INTEX-B) [*McNaughton*, 2008; *McNaughton et al.*, 2009].

[64] Figures 6 through 10 present the intensive aerosol optical properties of Asian plumes observed at MBO in the context of the other relevant data sets discussed above. As in Figure 5, the optical properties presented only represent periods when MBO was free from local BL influence.

[65] On average, the aerosol plumes observed at MBO had a higher submicrometer dry  $\omega$  than plumes observed closer to the Asian source region (Figure 6). The  $\sigma_{sp}$  measurements by *Anderson et al.* [2003] and *Yang et al.* [2009] were both made with a TSI integrating nephelometer so we can compare these measurements to those at MBO using the precision uncertainty; however, the  $\sigma_{ap}$  measurements were made with a single-wavelength PSAP. The average  $\omega$  value reported by *Anderson et al.* [2003] and that reported for MBO in Figure 6 are significantly different if the precision uncertainty is considered.

[66] The choice of correction scheme that is applied to the PSAP data will significantly impact the reported  $\omega$ . See auxiliary material Table S1 and section 2.2.2 for a discussion of the corrections schemes applied across the literature to PSAP data. If the MBO data presented in Figure 6 were corrected following either of the other two correction schemes cited in the literature, the  $\omega$  values would be larger and would constitute a larger increase compared to

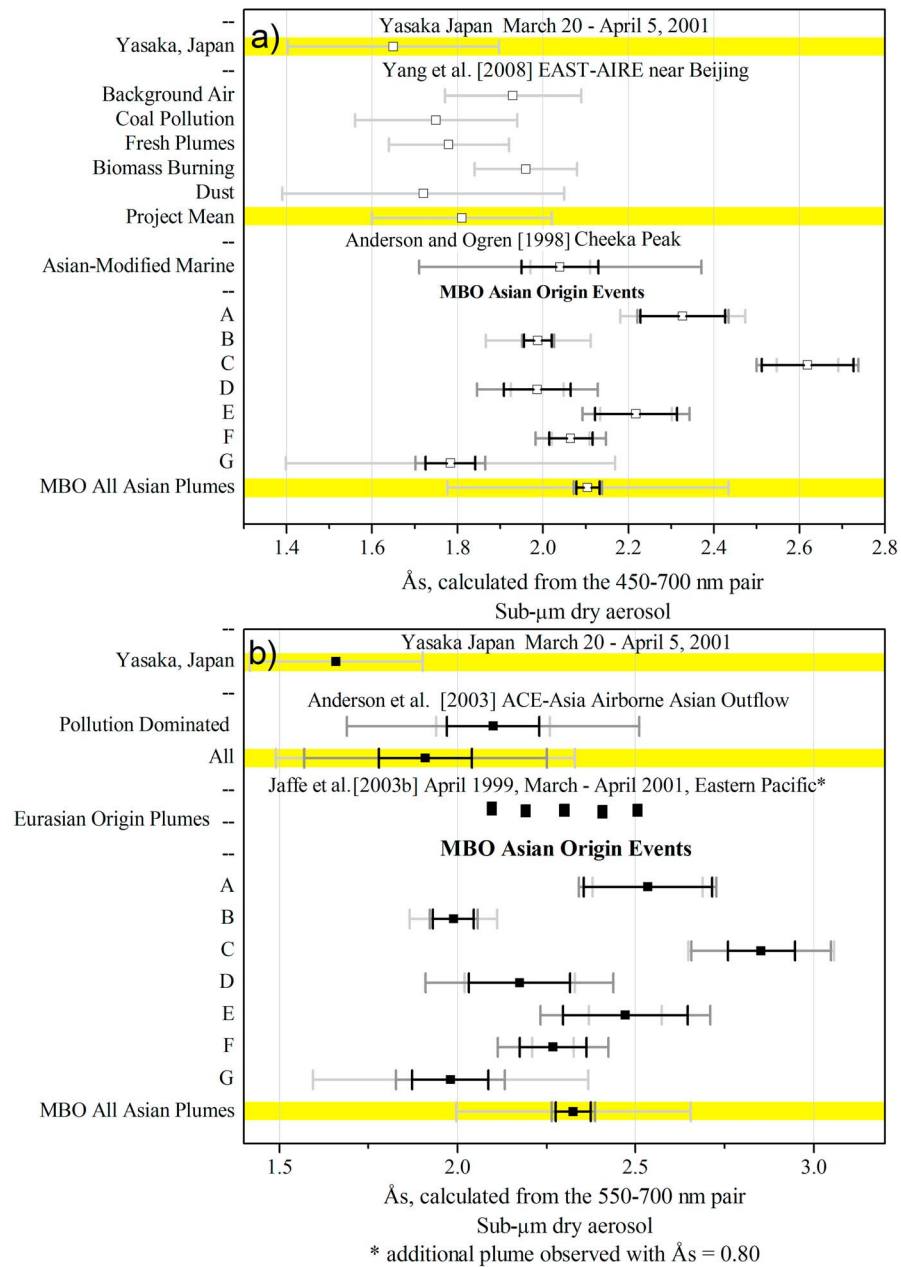


**Figure 8.** Comparison of the mean scattering Ångström exponent ( $\text{\AA}_s$ ) during Asian Origin aerosol plumes measured at MBO with other data sets. Light gray, dark gray and black bars are 1 standard deviation, the total uncertainty of the average, and the precision uncertainty of the average respectively. This plot does not include data from 1100–1900 Local Time when the local mixed layer may have been influencing MBO.

observations closer to the Asian source region. In other words, all correction schemes indicate that the submicrometer dry  $\omega$  values observed at MBO in Asian plumes are larger than those observed closer to the Asian source region, and the difference may be larger than inferred from Figure 6.

[67] Figure 7 presents the same set of data shown in Figure 6 as a function of processing time in the atmosphere. The horizontal axis presents the approximate times downwind from sources as aerosols move from Asia across the Pacific to North America. Yang et al. [2009] did not use back trajectories to identify specific emission sources

because of the density and proximity of sources. We have assigned a transport age of 0–2 days to this data set. The Asian outflow measurements from the ACE-Asia campaign presented by Quinn et al. [2004], Doherty et al. [2005], and Anderson et al. [2003] were assigned an approximate age of 1 to 4 days based on the discussion and back trajectories presented in these papers. See Figure 1 of Anderson et al. [2003] and Figure 1 of Quinn et al. [2004]. The McNaughton [2008] data were assigned an approximate age of 6–11 days based on the summary plot for the INTEX-B aircraft measurements presented by Dunlea et al. [2009]. Dunlea et al.

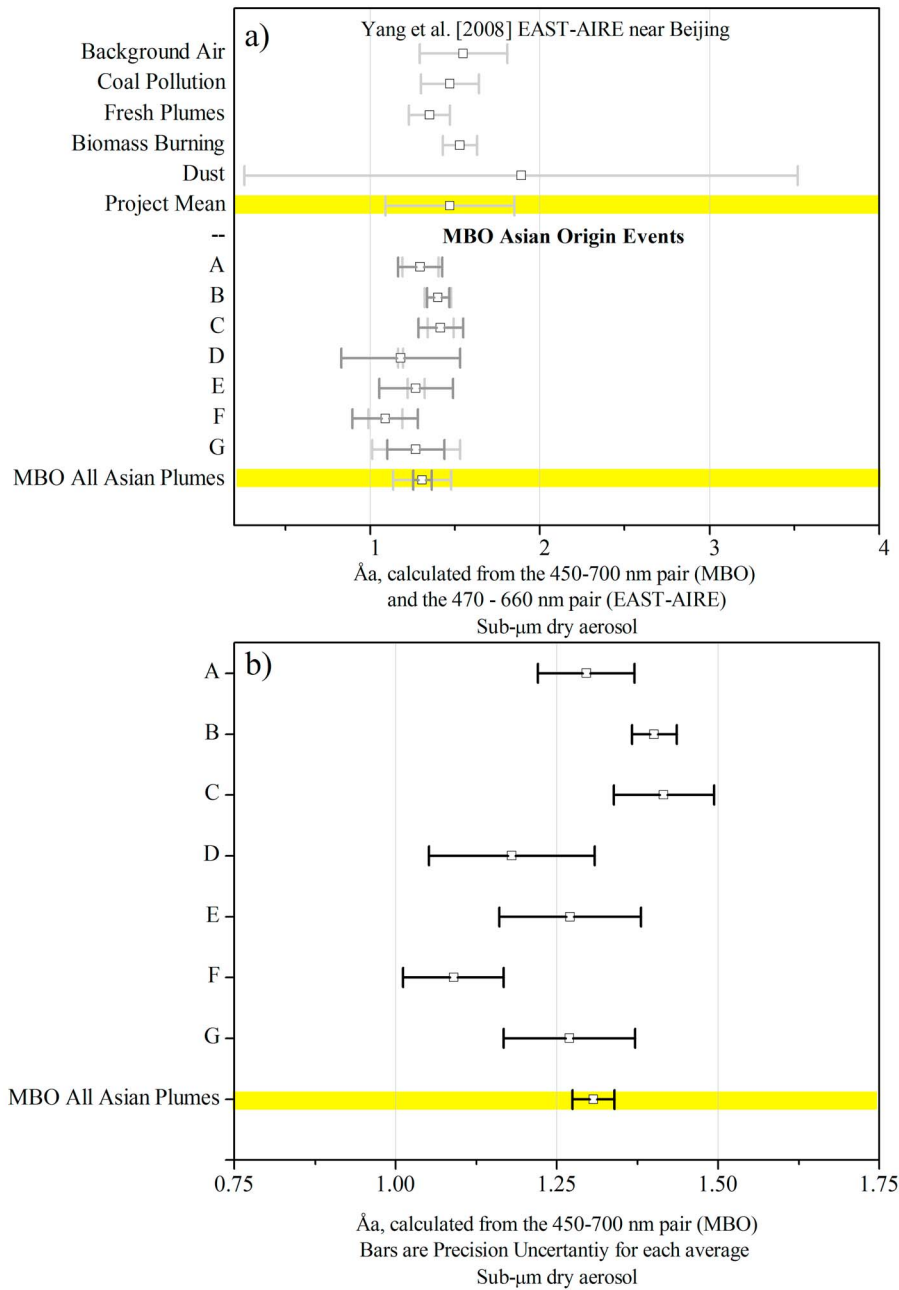


**Figure 9.** (a) Comparison of the absorption Ångström exponent ( $\text{\AA}_a$ ) during Asian Origin aerosol plumes measured at MBO during spring 2008 and spring 2009 with data from EAST-AIRE. Light gray and dark gray bars are 1 standard deviation and the total uncertainty of the average, respectively. This plot does not include data from 1100–1900 Local Time when the local mixed layer may have been influencing MBO. This work calculated  $\text{\AA}_a$  from the 450–700 nm pair, and it represents submicrometer aerosol only. *Yang et al.* [2009] calculated  $\text{\AA}_a$  from the 470–660 nm pair, and it represents all aerosol; there was no size cutoff. *Yang et al.* [2009] report the fine absorption fraction at 550 nm for each air mass type. The fine absorption fraction for dust and biomass burning was 0.69 and 0.80 respectively. It was 0.85 for both fresh chimney plumes and coal pollution. The project mean was 0.83. (b) Comparison of ( $\text{\AA}_a$ ) during Asian Origin aerosol plumes measured at MBO during spring 2008 and spring 2009. Bars are the precision uncertainty of the average for each plume.

[2009] present a summary figure for sulfate and organic aerosol processing as a function of processing time in the atmosphere. Asian plumes observed at MBO were assigned an approximate age based on the back trajectory calculations

and supporting satellite images. Figure 7 shows the increase of  $\omega$  with processing time in the atmosphere. This relationship appears to hold for the individual plumes observed at MBO as well.

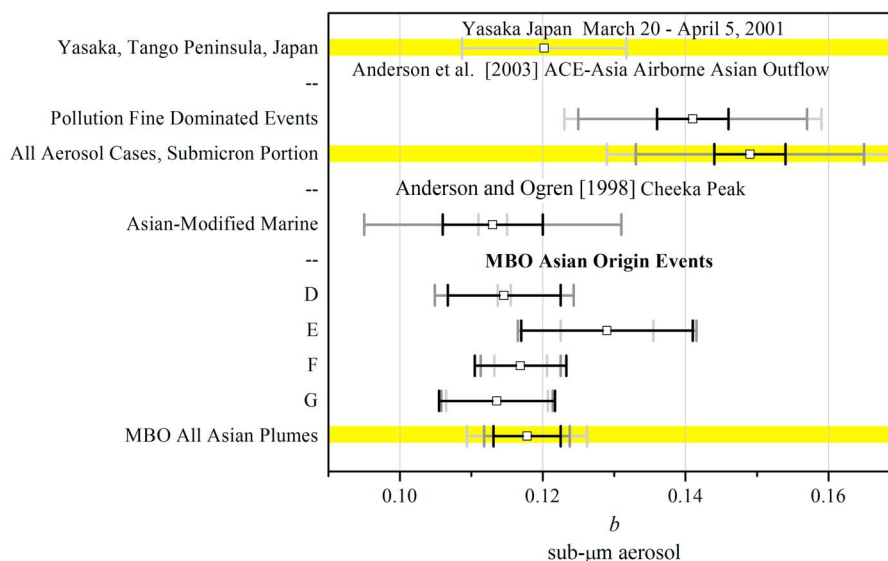


**Figure 10.** Comparison backscattering ratio ( $b$ ) during Asian Origin aerosol plumes measured at MBO during spring 2009 with other data sets. All values are reported at 550 nm. Light gray, dark gray, and black bars are 1 standard deviation, the total uncertainty of the average, and the precision uncertainty of the average, respectively. This plot does not include data from 1100–1900 Local Time when the local mixed layer may have been influencing MBO.

[68] The larger average aerosol  $\omega$  at MBO could be the result of either the addition of a coating of scattering material to the primary aerosols, or the in-transit formation of secondary aerosols. The addition of scattering material to an absorbing core during transpacific transport would increase both scattering and absorption through lensing of incident light [Bond and Bergstrom, 2006; Bond et al., 2006; Fuller et al., 1999]. The lensing effect is limited, but the scattering increase is not. The average  $\omega$  at MBO is larger than that observed in coal pollution and fresh plumes [Yang et al., 2009], but there is a relatively small difference between observations of aged Asian aerosol plumes observed at MBO and observations off the Asian coast [Anderson et al., 2003]. This suggests that the largest changes of  $\omega$  within aerosol plumes likely occur rapidly, on the time scale of a day.

[69] It should be noted that biomass burning plumes were not specifically identified by Anderson et al. [2003] or Quinn et al. [2004] in the ACE-Asia aerosol data. MBO plumes A, B and F likely all contain significant amounts of biomass burning smoke. The smoke in plumes A and B likely originated from a similar region (southeastern Russia) and therefore a similar fuel type; this was not the case for plume F which originated further west. The optical properties of aerosols from fires also change with particle size and black carbon content, both of which are dependent on combustion phase [Reid and Hobbs, 1998]. Smoke aerosols generally become less absorbing ( $\omega$  increases) over time as gases and water vapor condense onto the particles [Haywood et al., 2003], but with low-RH sampling at MBO, water is less important.

[70] The MBO  $\text{\AA}_s$  distributions (Figure 8) showed large plume-to-plume variability. From Figure 8 we can infer that there is a shift in the average aerosol size distribution toward smaller particles in the submicrometer distribution at MBO

compared to the Asian source region. We are referring here to the project means highlighted in yellow in Figure 8. Aside from Plume C, all the Asian plumes observed at MBO had a smaller average  $\text{\AA}_s$  than the North American pollution plume observed by Anderson et al. [1999] at Cheeka Peak (not shown in Figure 8).

[71] Brock et al. [2004] proposed a conceptual model for transpacific aerosol transport from Asia that could result in dramatic changes to the aerosol size distribution. During the first few days of transport downwind of Asia, gas-phase organic precursors form secondary organic aerosols (SOA) rapidly. This conversion is faster than the  $\text{SO}_2$  conversion to sulfate aerosols. Polluted air masses are then lifted out of the boundary layer within warm conveyor belts (WCBs) which are associated with moisture and clouds [Cooper et al., 2004]. The aerosols that have already formed when the air mass is lifted out of the boundary layer are washed out, while less-soluble gas-phase species (e.g.,  $\text{SO}_2$ ) are not entirely removed. The remaining gas-phase species are enhanced in  $\text{SO}_2$ , and sulfate forms in larger concentrations than SOA during transpacific transport [Brock et al., 2004]. This conceptual model is supported by recent observations of sulfate and organic aerosol in aged Asian pollution plumes encountered by the C-130 aircraft during INTEX-B in spring 2006 [Dunlea et al., 2009]. Dunlea et al. [2009] provided evidence for a shift in the sulfate size distribution overtime, but did not present the size distribution for the entire aerosol population. Their results showed a decrease in average particle size for a plume recently exported from the BL to the FT, followed by an increase in particle size with processing time during transpacific transport in the FT.

[72] However, there are a number of studies which appear inconsistent with the Brock et al. [2004] model. Observations of aerosols in the Northwest Pacific FT in 2001 showed high organic aerosol concentrations [Heald et al., 2005]. Further

downwind, an analysis of surface  $PM_{2.5}$  measurements from the U.S. IMPROVE network demonstrated that there is substantial loss and removal of sulfate in Asian plumes during transit across the Pacific [Jaffe *et al.*, 2005]. Dickerson *et al.* [2007] illustrated that dry convection plays an important role in the export of pollutants from the Asian continental BL to the FT. They show that WCBs are more important in cyclonic systems that have moved further east off the coast [Dickerson *et al.*, 2007]. These various BL-FT exchange mechanisms could be one source of the variability in  $\hat{A}_s$  we observed at MBO.

[73] Figure 9 indicates that the submicrometer aged Asian aerosols observed at MBO showed a strong spectral dependence on absorption, and the plume-to-plume variability was relatively small (refer to Table 2 for values). It should be noted that the  $\hat{A}_a$  distributions presented for EAST-AIRE in Figure 9a are not directly comparable to those presented for MBO because the EAST-AIRE observations represent all aerosol sizes and the multiwavelength absorption measurements were made with an aethelometer. However, limited relevant measurements of  $\hat{A}_a$  are available for a direct comparison. See the caption of Figure 9 for details. The range of  $\hat{A}_a$  values observed at MBO in aged Asian plumes is relatively small compared to reported observations of  $\hat{A}_a$  closer to sources [Bergstrom *et al.*, 2007; Yang *et al.*, 2009].

[74] Figure 10 indicates that plumes observed at MBO had a lower  $b$  than plumes observed closer to the Asian continent. Our data are self consistent, smaller particles are associated with stronger scattering in the backward hemisphere. However, the MBO results are not consistent with data collected closer to Asia. Figure 10 is difficult to interpret because it shows a decrease in the backscattering ratio between plumes observed at MBO and those observed closer to Asia. The results presented in Figure 8, and discussed previously in this section, suggest that on average there is a shift toward a smaller size distribution. Figure 5b confirms the expected inverse relationship between particle size and  $b$ . It is possible that the difference in  $b$  is driven by a change in the average particle shape more than the average particle size, and  $b$  is not a robust indicator of particle size. The mean  $b$  for plumes observed at MBO is  $\sim 20\%$  lower than that reported by Anderson *et al.* [2003] for Asian outflow intercepted by the C-130 during spring 2001. On the basis of our propagation of uncertainty, these differences are significant. However, Doherty *et al.* [2005] showed that we may not fully understand the precision uncertainty associated with the backscattering measurement in the TSI Model 3563 integrating nephelometer.

[75] We have compared observations of the intensive aerosol optical properties at MBO with those observed closer to the Asian source region in an attempt to better understand how the optical properties change with aerosol age. It should be noted that neither Anderson *et al.* [2003] or Quinn *et al.* [2004] made observations of Siberian biomass burning plumes, and there is strong evidence that such plumes were a major source of aerosols at MBO during spring 2008. Second Asian anthropogenic emissions of aerosols and their gas-phase precursors are dynamic, and the interannual variability is not well quantified. In terms of natural aerosol emissions, specifically dust, we know there can be large interannual variability in the dust source strength and that there is an impact on observed fine particulate concentra-

tions in the western United States [Fischer *et al.*, 2009]. For these reasons, multiple observations in a single plume would certainly be a better way to determine how the average optical properties of Asian aerosols change as they age. However, this type of data is not available at this time.

## 5. Conclusions and Recommendations for Future Work

[76] We present observations of aerosol optical properties associated with seven well-defined plumes of Asian origin observed at the MBO. When compared to literature observations, these measurements show a significant difference between the optical properties of aerosols over the western versus eastern Pacific. While we understand some aspects of why this is, more data are needed to fully understand this. Key results include the following.

[77] 1. Plumes of Asian origin included many of the highest  $\sigma_{sp}$  ( $34.8 \text{ Mm}^{-1}$  hourly average) and  $\sigma_{ap}$  ( $5.7 \text{ Mm}^{-1}$  hourly average) values observed at MBO over the 2008 and 2009 spring campaigns.

[78] 2. Intensive aerosol properties varied from plume to plume and within some of the plumes. This indicates that even after transpacific transport the aerosols are not necessarily well mixed and the plumes can be layered. It also reinforces the idea that each plume leaving Asia reflects a different mixture of sources.

[79] 3. The plumes clustered in terms of their optical properties. Plumes hypothesized to contain a large fraction of mineral dust were the most distinct, characterized by a relatively higher scattering Ångström ( $\hat{A}_s$ ) exponent.

[80] 4. On average the plume mean  $\hat{A}_s$  at MBO was larger than the project mean  $\hat{A}_s$  reported for both ACE-Asia aircraft aerosol observations and EAST-AIRE surface observations near Beijing. This suggests a shift toward smaller particles during transpacific transport. The plume-to-plume variability in  $\hat{A}_s$  could reflect different sources and/or various BL-FT exchange mechanisms.

[81] 5. The average submicrometer dry aerosol  $\omega$  observed in Asian plumes at MBO ( $0.88 \pm 0.01$ ) was slightly larger than mean observations closer to the Asian coast.

[82] 6. The average submicrometer dry aerosol  $b$  observed in Asian plumes at MBO ( $0.118 \pm 0.006$ ) was  $\sim 20\%$  smaller than mean observations closer to the Asian coast. This relationship is robust based on our current understanding of measurement uncertainties, but it is not fully understood.

[83] We have presented statistics on aerosol optical properties measured over two spring seasons (April–May) at one location in the lower free troposphere. Addressing the representativeness of observations at MBO would be a productive step toward using these results to address larger research questions such as the regional climate forcing of Asian aerosols. An obvious next step is to systematically connect observations at MBO with concurrent satellite observations to determine plume heights and horizontal extent. However, of the seven plumes presented here, only two (Plumes A and B) were well covered in terms of satellite observations [Thompson *et al.*, 2009] indicating that a longer data set is required for this type of analysis.

[84] Our results suggest a clear path forward for in situ aerosol observations at MBO. In addition to extending the optical measurements to include both the submicrometer

and supermicrometer aerosol fractions, we recommend adding measurements of aerosol chemical composition. Additional measurements of the appropriate chemical tracers could be used to determine if aged Asian smoke, pollution and dust aerosols can be stratified by their combined spectral scattering and absorption properties.

[85] We also need to improve our understanding of the relationship between size and  $b$  for nonspherical particles and particles with various mixing states. The interpretation of direct optical measurements of  $b$ , like those presented here, will continue to be challenging without a clear understanding of the measurement uncertainty and a better theoretical understanding.

[86] **Acknowledgments.** Emily V. Fischer was supported by a Department of Energy Graduate Research Environmental Fellowship. Support for Mount Bachelor Observatory was provided by the National Science Foundation under grant ATM-0724327. We would like to thank Dave Covert, Patricia Quinn, and Timothy Bates for helpful discussions on the material contained in this manuscript and Nels Laulainen for loaning us a PSAP during spring 2008. We also gratefully acknowledge the support provided by the Mount Bachelor maintenance staff.

## References

- Anderson, T. L., and J. A. Ogren (1998), Determining aerosol radiative properties using the TSI 3563 Integrating Nephelometer, *Aerosol Sci. Technol.*, *29*, 57–69, doi:10.1080/02786829808965551.
- Anderson, T. L., et al. (1996), Performance characteristics of a high-sensitivity, three-wavelength total scatter/backscatter nephelometer, *J. Atmos. Oceanic Technol.*, *13*, 967–986, doi:10.1175/1520-0426(1996)013<0967:PCOAHS>2.0.CO;2.
- Anderson, T. L., D. Covert, J. D. Wheeler, J. M. Harris, K. D. Perry, B. Trost, D. Jaffe, and J. A. Ogren (1999), Aerosol backscatter fraction and single scattering albedo: Measured values and uncertainties at a coastal station in the Pacific Northwest, *J. Geophys. Res.*, *104*(D21), 26,793–26,807, doi:10.1029/1999JD900172.
- Anderson, T. L., S. J. Masonis, D. Covert, N. C. Ahlquist, S. Howell, A. D. Clarke, and C. McNaughton (2003), Variability of aerosol optical properties derived from in situ aircraft measurements during ACE-Asia, *J. Geophys. Res.*, *108*(D23), 8647, doi:10.1029/2002JD003247.
- Ångström, A. K. (1929), On the atmospheric transmission of Sun radiation and on dust in the air, *Geogr. Ann.*, *11*, 156–166.
- Bergstrom, R. W., P. Pilewskie, P. B. Russell, J. Redemann, T. C. Bond, P. K. Quinn, and B. Sierau (2007), Spectral absorption properties of atmospheric aerosols, *Atmos. Chem. Phys.*, *7*, 5937–5943, doi:10.5194/acp-7-5937-2007.
- Berner, A., C. H. Lurzer, F. Pohl, O. Preining, and P. Wagner (1979), The size distribution of the urban aerosol in Vienna, *Sci. Total Environ.*, *13*, 245–261, doi:10.1016/0048-9697(79)90105-0.
- Bond, T. C., and R. W. Bergstrom (2006), Light absorption by carbonaceous particles: An investigative review, *Aerosol Sci. Technol.*, *40*, 27–67, doi:10.1080/02786820500421521.
- Bond, T. C., T. L. Anderson, and J. R. Campbell (1999), Calibration and intercomparison of filter-based measurements of visible light absorption by particles, *Aerosol Sci. Technol.*, *30*, 582–600, doi:10.1080/027868299304435.
- Bond, T. C., G. Habib, and R. W. Bergstrom (2006), Limitations in the enhancement of visible light absorption due to mixing state, *J. Geophys. Res.*, *111*, D20211, doi:10.1029/2006JD007315.
- Boren, C. F., and D. R. Huffman (1983), *Absorption and Scattering of Light by Small Particles*, John Wiley, Hoboken, N. J.
- Brock, C. A., et al. (2004), Particle characteristics following cloud-modified transport from Asia to North America, *J. Geophys. Res.*, *109*, D23S26, doi:10.1029/2003JD004198.
- Carmichael, G. R., et al. (2009), Asian aerosols: Current and year 2030 distributions and implications to human health and regional climate change, *Environ. Sci. Technol.*, *43*, 5811–5817, doi:10.1021/es8036803.
- Carrico, C. M., P. Kus, M. J. Rood, P. K. Quinn, and T. S. Bates (2003), Mixtures of pollution, dust, sea salt, and volcanic aerosol during ACE-Asia: Radiative properties as a function of relative humidity, *J. Geophys. Res.*, *108*(D23), 8650, doi:10.1029/2003JD003405.
- Chin, M., T. Diehl, P. Ginoux, and W. C. Malm (2007), Intercontinental transport of pollution and dust aerosols: Implications for regional air quality, *Atmos. Chem. Phys.*, *7*, 5501–5517, doi:10.5194/acp-7-5501-2007.
- Clarke, A., et al. (2007), Biomass burning and pollution aerosol over North America: Organic components and their influence on spectral optical properties and humidification response, *J. Geophys. Res.*, *112*, D12S18, doi:10.1029/2006JD007777.
- Cooper, O. R., et al. (2004), A case study of transpacific warm conveyor belt transport: Influence of merging airstreams on trace gas import to North America, *J. Geophys. Res.*, *109*, D23S08, doi:10.1029/2003JD003624.
- DeBell, L. J., M. Vozella, R. W. Talbot, and J. E. Dibb (2004), Asian dust storm events of spring 2001 and associated pollutants observed in New England by the Atmospheric Investigation, Regional Modeling, Analysis and Prediction (AIRMAP) monitoring network, *J. Geophys. Res.*, *109*, D01304, doi:10.1029/2003JD003733.
- Dickerson, R. R., et al. (2007), Aircraft observations of dust and pollutants over northeast China: Insight into the meteorological mechanisms of transport, *J. Geophys. Res.*, *112*, D24S90, doi:10.1029/2007JD008999.
- Diner, D. J., et al. (2004), PARAGON: An integrated approach for characterizing aerosol climate impacts and environmental interactions, *Bull. Am. Meteorol. Soc.*, *85*(10), 1491–1501, doi:10.1175/BAMS-85-10-1491.
- Doherty, S., P. K. Quinn, A. Jefferson, C. M. Carrico, T. L. Anderson, and D. A. Hegg (2005), A comparison and summary of aerosol properties as observed in situ from aircraft, ship, and land during ACE-Asia, *J. Geophys. Res.*, *110*, D04201, doi:10.1029/2004JD004964.
- Draxler, R. R., and G. D. Hess (1998), An overview of the HYSPLIT\_4 modelling system for trajectories, dispersion, and deposition, *Aust. Meteorol. Mag.*, *47*, 295–308.
- Duncan, B. N., R. V. Martin, A. C. Staudt, R. Yevich, and J. A. Logan (2003), Interannual and seasonal variability of biomass burning emissions constrained by satellite observations, *J. Geophys. Res.*, *108*(D2), 4100, doi:10.1029/2002JD002378.
- Dunlea, E. J., et al. (2009), Evolution of Asian aerosols during transpacific transport in INTEX-B, *Atmos. Chem. Phys.*, *9*, 7257–7287, doi:10.5194/acp-9-7257-2009.
- Echalar, F., A. Caudichet, H. Cachier, and P. Artaxo (1995), Aerosol emissions by tropical forest and savanna biomass burning: Characteristic trace elements and fluxes, *Geophys. Res. Lett.*, *22*(22), 3039–3042, doi:10.1029/95GL03170.
- Fialho, P., A. D. A. Hansen, and R. E. Honrath (2005), Absorption coefficients by aerosols in remote areas: A new approach to decouple dust and black carbon absorption coefficients using seven-wavelength Aethalometer data, *J. Aerosol Sci.*, *36*(2), 267–282, doi:10.1016/j.jaerosci.2004.09.004.
- Fischer, E. V., N. C. Hsu, D. A. Jaffe, M.-J. Jeong, and S. L. Gong (2009), A decade of dust: Asian dust and springtime aerosol load in the U.S. Pacific Northwest, *Geophys. Res. Lett.*, *36*, L03821, doi:10.1029/2008GL036467.
- Fischer, E. V., D. A. Jaffe, D. R. Reidmiller, and L. Jaeglé (2010), Meteorological controls on observed peroxyacetyl nitrate (PAN) at Mount Bachelor during the spring of 2008, *J. Geophys. Res.*, *115*, D03302, doi:10.1029/2009JD012776.
- Fuller, K. A., W. C. Malm, and S. M. Kreidenweis (1999), Effects of mixing on extinction by carbonaceous particles, *J. Geophys. Res.*, *104*(D13), 15,941–15,954, doi:10.1029/1998JD100069.
- Gaudichet, A., F. Echalar, B. Chatenet, J. P. Quisefit, G. Malingre, H. Cachier, P. Baut-Menard, P. Artaxo, and W. Maenhaut (1995), Trace elements in tropical African savanna biomass burning aerosols, *J. Atmos. Chem.*, *22*, 19–39, doi:10.1007/BF00708179.
- Haywood, J. M., and K. P. Shine (1995), The effect of anthropogenic sulfate and soot aerosol on the clear-sky planetary radiation budget, *Geophys. Res. Lett.*, *22*(5), 22,603–22,606.
- Haywood, J. M., S. R. Osborne, P. N. Francis, A. Keil, P. Formenti, M. O. Andreae, and P. H. Kaye (2003), The mean physical and optical properties of regional haze dominated by biomass burning aerosol measured from the C-130 aircraft during SAFARI 2000, *J. Geophys. Res.*, *108*(D13), 8473, doi:10.1029/2002JD002226.
- Heald, C. L., D. J. Jacob, R. J. Park, L. Russell, B. J. Hubert, J. H. Seinfeld, H. Liao, and R. J. Weber (2005), A large organic aerosol source in the free troposphere missing from current models, *Geophys. Res. Lett.*, *32*, L18809, doi:10.1029/2005GL023831.
- Heald, C. L., D. J. Jacob, R. J. Park, B. Alexander, T. D. Fairlie, R. M. Yantosca, and D. A. Chu (2006), Transpacific transport of Asian anthropogenic aerosols and its impact on surface air quality in the United States, *J. Geophys. Res.*, *111*, D14310, doi:10.1029/2005JD006847.
- Heintzenberg, J., and R. J. Charlson (1996), Design and applications of the integrating nephelometer: A review, *J. Atmos. Oceanic Technol.*, *13*, 987–1000, doi:10.1175/1520-0426(1996)013<0987:DAAOTI>2.0.CO;2.

- Huebert, B. J., T. S. Bates, P. B. Russell, G. Shi, Y. J. Kim, K. Kawamura, G. R. Carmichael, and T. Nakajima (2003), An overview of ACE-Asia: Strategies for quantifying the relationships between Asian aerosols and their climatic impacts, *J. Geophys. Res.*, *108*(D23), 8633, doi:10.1029/2003JD003550.
- Husar, R. B., et al. (2001), Asian dust events of April 1998, *J. Geophys. Res.*, *106*(D16), 18,317–18,330, doi:10.1029/2000JD900788.
- Intergovernmental Panel on Climate Change (IPCC) (2007), *Climate Change 2007: The Physical Science Basis, Working Group I Contribution to the Fourth Assessment*, edited by S. Solomon et al., Cambridge Univ. Press, Cambridge, U. K.
- Jaffe, D. A., et al. (1999), Transport of Asian air pollution to North America, *Geophys. Res. Lett.*, *26*(6), 711–714, doi:10.1029/1999GL001000.
- Jaffe, D. A., J. A. Snow, and O. R. Cooper (2003a), Asian dust events: Transport and impact on surface aerosol concentrations in the United States, *Eos Trans. AGU*, *84*(46), 501, doi:10.1029/2003EO460001.
- Jaffe, D. A., I. McKendry, T. Anderson, and H. Price (2003b), Six ‘new’ episodes of trans-Pacific transport of air pollutants, *Atmos. Environ.*, *37*, 391–404, doi:10.1016/S1352-2310(02)00862-2.
- Jaffe, D. A., I. Bertschi, L. Jaegle, P. Novelli, J. S. Reid, H. Tanimot, R. Vingarzan, and D. L. Westphal (2004), Long-range transport of Siberian biomass burning emissions and impact on surface ozone in western North America, *Geophys. Res. Lett.*, *31*, L16106, doi:10.1029/2004GL020093.
- Jaffe, D. A., S. Tamura, and J. Harris (2005), Seasonal cycle and composition of background fine particles along the west coast of the US, *Atmos. Environ.*, *39*, 297–306, doi:10.1016/j.atmosenv.2004.09.016.
- Kalashnikova, O. V., and I. N. Sokolik (2002), Importance of shapes and composition of wind-blown dust particles for remote sensing at solar wavelengths, *Geophys. Res. Lett.*, *29*(10), 1398, doi:10.1029/2002GL014947.
- Kaufman, Y. J., D. Tanré, and O. Boucher (2002), A satellite view of aerosols in the climate system, *Nature*, *419*, 215–223, doi:10.1038/nature01091.
- Lack, D. A., C. D. Cappa, D. S. Covert, T. Baynard, P. Massoli, B. Sierau, T. S. Bates, P. K. Quinn, E. R. Lovejoy, and A. R. Ravishankara (2008), Bias in filter-based aerosol light absorption measurements due to organic aerosol loading: Evidence from ambient measurements, *Aerosol Sci. Technol.*, *42*, 1033–1041, doi:10.1080/02786820802389277.
- Lack, D. A., C. D. Cappa, E. S. Cross, P. Massoli, A. T. Ahern, P. Davidovits, and T. B. Onasch (2009), Absorption enhancement of coated absorbing aerosols: Validation of the photo-acoustic technique for measuring the enhancement, *Aerosol Sci. Technol.*, *43*, 1006–1012, doi:10.1080/02786820903117932.
- Lapina, K., R. E. Honrath, R. C. Owen, M. Val Martin, and G. Pfister (2006), Evidence of significant large-scale impacts of boreal fires on ozone levels in the midlatitude Northern Hemisphere free troposphere, *Geophys. Res. Lett.*, *33*, L10815, doi:10.1029/2006GL025878.
- Liu, Z. Y., M. Vaughan, D. Winker, C. Kittaka, B. Getzewich, R. Kuehn, A. Omar, K. Powell, C. Trepte, and C. Hosteller (2009), The CALIPSO lidar cloud and aerosol discrimination: Version 2 algorithm and initial assessment of performance, *J. Atmos. Oceanic Technol.*, *26*, 1198–1213, doi:10.1175/2009JTECHA1229.1.
- Malm, W. C., J. F. Sisler, D. Huffman, R. A. Eldred, and T. A. Cahill (1994), Spatial and seasonal trends in particle concentration and optical extinction in the United States, *J. Geophys. Res.*, *99*(D1), 1347–1370.
- Marshall, S. F., D. S. Covert, and R. J. Charlson (1995), Relationship between asymmetry parameter and hemispheric backscatter ratio: Implications for climate forcing by aerosols, *Appl. Opt.*, *34*(27), 6306–6311, doi:10.1364/AO.34.006306.
- McNaughton, C. S. (2008), Constraining climate model simulations of aerosol size distributions over the North Pacific and North America using in-situ airborne measurements, Ph. D. thesis, Univ. of Hawaii at Manoa, Honolulu.
- McNaughton, C. S., et al. (2009), Observations of heterogeneous reactions between Asian pollution and mineral dust over the Eastern North Pacific during INTEX-B, *Atmos. Chem. Phys.*, *9*, 8283–8308, doi:10.5194/acp-9-8283-2009.
- Morris, G. A., et al. (2006), Alaskan and Canadian forest fires exacerbate ozone pollution over Houston, Texas, on 19 and 20 July 2004, *J. Geophys. Res.*, *111*, D24503, doi:10.1029/2006JD007090.
- Omar, A. H., J.-G. Won, D. Winker, S.-C. Yoon, O. Dubovik, and M. P. McCormick (2005), Development of global aerosol models using cluster analysis of Aerosol Robotic Network (AERONET) measurements, *J. Geophys. Res.*, *110*, D10S14, doi:10.1029/2004JD004874.
- Omar, A. H., et al. (2009), The CALIPSO automated aerosol classification and lidar ratio selection algorithm, *J. Atmos. Oceanic Technol.*, *26*, 1994–2014, doi:10.1175/2009JTECHA1231.1.
- Patterson, E. M. (1981), Optical properties of crustal aerosol: Relation to chemical and physical characteristics, *J. Geophys. Res.*, *86*(C4), 3236–3246, doi:10.1029/JC086iC04p03236.
- Price, H. U., D. Jaffe, O. R. Cooper, and P. V. Doskey (2004), Photochemistry, ozone production, and dilution during long-range transport episodes from Eurasia to the northwest United States, *J. Geophys. Res.*, *109*, D23S13, doi:10.1029/2003JD004400.
- Quinn, P. K., et al. (2004), Aerosol optical properties measured on board the Ronald H. Brown during ACE-Asia as a function of aerosol chemical composition and source region, *J. Geophys. Res.*, *109*, D19S01, doi:10.1029/2003JD004010.
- Reid, J. S., and P. V. Hobbs (1998), Physical and optical properties of young smoke from individual biomass fires in Brazil, *J. Geophys. Res.*, *103*(D24), 32,013–32,031, doi:10.1029/98JD00159.
- Reid, J. S., R. Koppmann, T. F. Eck, and D. P. Eleuterio (2004), A review of biomass burning emissions part II: Intensive physical properties of biomass burning particles, *Atmos. Chem. Phys. Discuss.*, *4*, 5135–5200, doi:10.5194/acpd-4-5135-2004.
- Reid, J. S., T. F. Eck, S. A. Christopher, R. Koppmann, O. Dubovik, D. P. Eleuterio, B. N. Holben, E. A. Reid, and J. Zhang (2005), A review of biomass burning emissions part III: Intensive optical properties of biomass burning particles, *Atmos. Chem. Phys. Discuss.*, *5*, 827–849.
- Reidmiller, D. R., D. A. Jaffe, E. V. Fischer, and B. Finley (2010), Nitrogen oxides in the boundary layer and free troposphere at the Mt. Bachelor Observatory, *Atmos. Chem. Phys. Discuss.*, *10*, 5751–5801, doi:10.5194/acpd-10-5751-2010.
- Rockström, J., et al. (2009), A safe operating space for humanity, *Nature*, *461*, 472–475, doi:10.1038/461472a.
- Sheridan, P. J., et al. (2005), The Reno Aerosol Optics Study: An evaluation of aerosol absorption measurement methods, *Aerosol Sci. Technol.*, *39*, 1–16, doi:10.1080/027868290901891.
- Sierau, B., D. S. Covert, D. J. Coffman, P. K. Quinn, and T. S. Bates (2006), Aerosol optical properties during the 2004 New England Air Quality Study—Intercontinental Transport and Chemical Transformation: Gulf of Maine surface measurements—Regional and case studies, *J. Geophys. Res.*, *111*, D23S37, doi:10.1029/2006JD007568.
- Subramanian, R., C. A. Roden, P. Boparai, and T. C. Bond (2007), Yellow beads and missing particles: Trouble ahead for filter based absorption measurements, *Aerosol Sci. Technol.*, *41*, 630–637, doi:10.1080/02786820701344589.
- Thompson, R. S., E. V. Fischer, D. A. Jaffe, and M. Di Perro (2009), Integrating MISR, MODIS, and CALIPSO satellite data with in situ measurements at Mount Bachelor to determine aerosol plume characteristics, *Eos Trans. AGU*, *90*(52), Fall Meet. Suppl., Abstract A33B-0246.
- VanCuren, R. A. (2003), Asian aerosols in North America: Extracting the chemical composition and mass concentration of the Asian continental aerosol plume from long-term aerosol records in the western United States, *J. Geophys. Res.*, *108*(D20), 4623, doi:10.1029/2003JD003459.
- VanCuren, R. A., and T. A. Cahill (2002), Asian aerosols in North America: Frequency and concentration of fine dust, *J. Geophys. Res.*, *107*(D24), 4804, doi:10.1029/2002JD002204.
- Viana, M., et al. (2008), Tracers and impact of open burning of rice straw residues on PM in eastern Spain, *Atmos. Environ.*, *42*, 1941–1957, doi:10.1016/j.atmosenv.2007.11.012.
- Virkkula, A., N. C. Ahlquist, D. S. Covert, W. P. Arnott, P. J. Sheridan, P. K. Quinn, and D. J. Coffman (2005), Modification, calibration and field test of an instrument for measuring light absorption by particles, *Aerosol Sci. Technol.*, *39*, 68–83, doi:10.1080/027868290901963.
- Warneke, C., et al. (2009), Biomass burning in Siberia and Kazakhstan as an important source for haze over the Alaskan Arctic in April 2008, *Geophys. Res. Lett.*, *36*, L02813, doi:10.1029/2008GL036194.
- Weiss-Penzias, P., D. Jaffe, P. Swartzendruber, J. B. Dennison, D. Chand, W. Hafner, and E. Prestbo (2006), Observations of Asian air pollution in the free troposphere at Mount Bachelor Observatory during spring of 2004, *J. Geophys. Res.*, *111*, D10304, doi:10.1029/2005JD006522.
- Weiss-Penzias, P., D. Jaffe, P. Swartzendruber, W. Hafner, D. Chand, and E. Prestbo (2007), Quantifying atmospheric mercury emissions from biomass burning and East Asian industrial regions based on ratios with carbon monoxide in pollution plumes at the Mount Bachelor Observatory, *Atmos. Environ.*, *41*, doi:10.1016/j.atmosenv.2007.1001.1058.
- Westerling, A. L., A. Gershunov, T. J. Brown, D. R. Cayan, and M. D. Dettinger (2003), Climate and wildfire in the western United States, *Bull. Am. Meteorol. Soc.*, *84*(5), 595–604, doi:10.1175/BAMS-84-5-595.
- Wuebbles, D. J., H. Lei, and J. Lin (2007), Intercontinental transport of aerosols and photochemical oxidants from Asia and its consequences, *Environ. Pollut.*, *150*, 65–84, doi:10.1016/j.envpol.2007.06.066.
- Yang, M., S. G. Howell, J. Zhuang, and B. J. Huebert (2009), Attribution of aerosol light absorption to black carbon, brown carbon, and dust in China—Interpretations of atmospheric measurements during EAST-AIRE, *Atmos. Chem. Phys.*, *9*, 2035–2050, doi:10.5194/acp-9-2035-2008.

Yu, H., L. A. Remer, M. Chin, H. Bian, R. G. Kleidman, and T. Diehl (2008), A satellite-based assessment of transpacific transport of pollution aerosol, *J. Geophys. Res.*, *113*, D14S12, doi:10.1029/2007JD009349.

---

E. Fischer and D. A. Jaffe, Department of Atmospheric Sciences, University of Washington, 408 ATG Bldg., Box 351640, Seattle, WA 98195, USA. (efischer@atmos.washington.edu)

J. S. Gaffney, Department of Chemistry, University of Arkansas at Little Rock, Little Rock, AR 72204, USA.

A. Marchany-Rivera, Department of Applied Science, University of Arkansas at Little Rock, Little Rock, AR 72204, USA.

N. A. Marley, Graduate Institute of Technology, University of Arkansas at Little Rock, Little Rock, AR 72204, USA.